Astronomy & Astrophysics manuscript no. NewBinaries
July 12, 2021

The post-common envelope central stars of the planetary nebulae Henize 2-155 and Henize 2-161⋆

D. Jones[1,2], H.M.J. Boffin[3], P. Rodríguez-Gil[1,2], R. Wesson[3], R.L.M. Corradi[1,2], B. Miszalski[4,5], and S. Mohamed[4]

[1] Instituto de Astrofísica de Canarias, E-38200 La Laguna, Tenerife, Spain
e-mail: djones@iac.es
[2] Departamento de Astrofísica, Universidad de La Laguna, E-38206 La Laguna, Tenerife, Spain
[3] European Southern Observatory, Alonso de Córdova 3107, Casilla 19001, Santiago, Chile
[4] South African Astronomical Observatory, P.O. Box 9, Observatory, 7935 Cape Town, South Africa
[5] Southern African Large Telescope Foundation, P.O. Box 9, Observatory, 7935 Cape Town, South Africa

Received 3 December 2014 / accepted ? ??? 2015

ABSTRACT

We present a study of Hen 2-155 and Hen 2-161, two planetary nebulae which bear striking morphological similarities to other planetary nebulae known to host close-binary central stars. Both central stars are revealed to be photometric variables while spectroscopic observations confirm that Hen 2-155 is host to a double-eclipsing, post-common-envelope system with an orbital period of 3^h33^m making it one of the shortest period binary central stars known. The observations of Hen 2-161 are found to be consistent with a post-common-envelope binary of period ∼1 day.

A detailed model of central star of Hen 2-155, is produced, showing the nebular progenitor to be a hot, post-AGB remnant of approximately 0.62 $M_\odot$, consistent with the age of the nebula, and the secondary star to be an M dwarf whose radius is almost twice the expected ZAMS radius for its mass. In spite of the small numbers, all main-sequence companions, of planetary nebulae central stars, to have had their masses and radii constrained by both photometric and spectroscopic observations have also been found to display this "inflation". The cause of the "inflation" is uncertain but is probably related to rapid accretion, immediately before the recent common-envelope phase, to which the star has not yet thermally adjusted.

The chemical composition of both nebulae is also analysed, showing both to display elevated *abundance discrepancy factors*. This strengthens the link between elevated *abundance discrepancy factors* and close binarity in the nebular progenitor.

Key words. planetary nebulae: individual: Hen 2-155 - planetary nebulae: individual: Hen 2-161 - Stars: binaries: close - Stars: binaries: eclipsing - Stars: circumstellar matter - Stars: AGB and post-AGB ISM: abundances

1. Introduction

Planetary nebulae (PNe) with close binary central stars offer an important laboratory for the study of binary evolution - in particular, the poorly understood common envelope (CE) phase. To date, approximately 50 close binary central stars (hereafter bCSPNe - binary central stars of PNe) have been discovered[1] (Miszalski et al. 2009a; de Marco et al. 2008; Boffin 2014b) with many more expected (given the high binary fraction amongst those nebulae observed by photometric surveys, e.g. Miszalski et al. 2009a; Bond 2000). Finding, and accurately constraining the orbital parameters of, these missing binaries is a time consuming task, with a completely unbiased survey requiring many, many nights of photometric monitoring and subsequent spectroscopic follow-up. As such, it is more reasonable to use the morphological features identified by Miszalski et al. (2009b), as being particularly prevalent amongst PNe with binary central stars, as selection criteria for targeted photometric searches for new binaries. These features include filamentary structures, rings, polar outflows and bipolarity, and have been successfully employed by our group in the discovery of several new binary central stars (Miszalski et al. 2011a,b; Corradi et al. 2011; Boffin et al. 2012b; Jones et al. 2014a; Santander-García et al. 2015).

Here, we report on the discovery of post-common envelope central stars at the heart of the PNe Hen 2-155 and Hen 2-161, two nebulae selected for study based on their similar appearance to other PNe known to host binary central stars. We also highlight the novel use of narrowband filters in our photometric monitoring, which afford the possibility to study some of the bright nebulae previously inaccessible to broadband photometric methods.

Hen 2-155 ($\alpha = 16^h19^m23.17^s$, $\delta = -42°15'36.64''$, PN G338.8+05.6) and Hen 2-161 ($\alpha = 16^h24^m37.79^s$, $\delta = -53°22'34.14''$, PN G331.5−02.7) were both discovered by Karl G. Henize in 1967, forming part of his catalogue of Southern planetary nebulae (Henize 1967). Both PNe display elongated (following the classification scheme of Sahai et al. 2011) morphologies with knotty filamentary waists, typical of those PNe already known to host binary central stars. Beyond this initial similarity, both nebulae are remarkably similar to some of the most interesting examples in the currently known sample and were, therefore, selected by our group for study.

The wispy extensions and irregular central filaments of Hen 2-155 (see figure 1) are extremely similar to those found in NGC 6326, NGC 6778, Hen 2-11, and NGC 5189 (Miszalski et al. 2011b; Jones et al. 2014a; Manick et al. 2015). The geometrically opposed pairs of "knots" seen marking the

⋆ Tables of photometry and radial velocity measurements available at the CDS via anonymous ftp to cdsarc.u-strasbg.fr

[1] http://drdjones.net/bCSPN

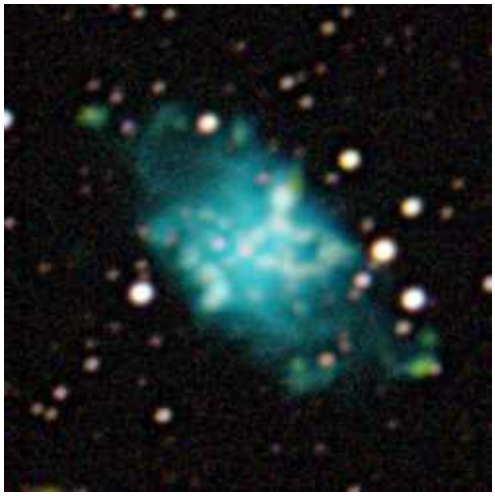

Fig. 1. Colour composite image of Hen 2-155 (for exposures in individual filters please see figure 3). North is up, East is to the left. The image measures 1′×1′.

ends of the major axis of the nebula are relatively typical of high velocity outflows or "jets" which are believed to be typical of central star binarity. Of additional interest, the central binaries of NGC 6326, NGC 6778 and Hen 2-11 all display extremely strong photometric variability and periods shorter than 1 day (much shorter in the case of NGC 6778 at 0.1534 day), making for relatively easy detection, whilst Hen 2-11 and NGC 6778 are known to host eclipsing systems. Eclipses are key in measuring accurate and model independent masses (Miszalski et al. 2008), which are, in turn, extremely important in accurately constraining the state of these binaries upon exiting the CE. The presence of the PN ensures that the system is "fresh out of the oven" as the nebula itself is the product of the ejection of the CE, and the lifetime of the PN is insufficient for significant changes to have occurred in the binary post-ejection.

Hen 2-161 shows a knotty equatorial ring forming the waist of an elongated, possibly bipolar, morphology (figure 2 of this paper, and figure 3 lower panel of Sahai et al. 2011) reminiscent of the morphology of The Necklace (figure 2), as well as several other post-CE PNe (e.g. Sab 41, Miszalski et al. 2009b; and Fg 1, Boffin et al. 2012b). Once again, the central binary of The Necklace shows extremely strong variability and a relatively short period (1.16 day, Corradi et al. 2011), but is of special interest due to the chemical peculiarity of the companion star in the system. The secondary in The Necklace has been shown to be a Carbon Dwarf star, indicating that it has been chemically polluted (with AGB material) by the primary star - thus far the only direct evidence of mass transfer during or, much more likely, just prior to the CE phase in a PN (Miszalski et al. 2013). Additionally, the central star of Hen 2-161 has been shown to be displaced from the geometric centre of the nebula (Sahai et al. 2011), another possible indicator of central star binarity (Soker et al. 1998).

A summary of the known parameters, stellar and nebular, of both Hen 2-155 and Hen 2-161 can be found in table 1.

The paper is structured as follows. Sect. 2 outlines the observations and data reduction, Sect. 3 describes the light curve analysis and modelling, and the analysis of the stellar and nebular spectroscopy. Finally, Sect. 4 discusses the results.

Table 1. Parameters, both stellar and nebular, of Hen 2-155 and Hen 2-161 from the literature

	Hen 2-155	Hen 2-161	References
Reddening, $c(H_\beta)$	0.81–1.01	0.35–1.80	1,2
Distance (kpc)	2.47–3.15	3.64–5.31	3,4
Central star temperature estimate(s) (kK)	T_Z(H)=51 T_Z(He II)=73	T_{EB}=35.1	5,6
Nebular systemic velocity (km s^{-1})	-35.3±15.0	-98.0±9.0	7
Approximate nebular diameter (″)	14.5–16.9[a]	9.7–16.3	8

References. (1) Cavichia et al. (2010); (2) Cahn et al. (1992); (3) Phillips (2004); (4) Stanghellini et al. (2008); (5) Kaler & Jacoby (1991); (6) Preite-Martinez et al. (1989) ; (7) Durand et al. (1998); (8) Tylenda et al. (2003).

Notes. [(a)] This measurement encompasses the "waist" of the nebula but not the wispy extensions which reach out to ∼30″ from the central star.

2. Observations and data reduction

2.1. Photometry

Photometric monitoring of the central stars of Hen 2-155 and Hen 2-161 was carried out using the EFOSC2 instrument on the 3.6-m ESO-NTT (Buzzoni et al. 1984; Snodgrass et al. 2008). The observations employed the E2V CCD with a pixel scale of 0.24″×0.24″ pixel^{-1}. Hen 2-155 was observed with the Hβ-continuum filter (#743) on the nights of February 27–29, March 1–2 2012, and February 23–26 2014, while Hen 2-161 was observed with the Gunn *i* filter (#705) on the nights of February 29, March 1–2 2012, January 14–15, June 2–6 2013, and February 23–26 2014. For both objects, the exposure time was varied in order to ensure a sufficiently high signal-to-noise ratio in the resulting images (for a full list of individual exposures, see tables 2 and 3 available in the online material). All data were debiased and flat-fielded using standard STARLINK routines[2].

Narrowband emission line images of both objects were also acquired with EFOSC2 and the following filters: Hα (# 692, includes [N II] λ6548 Å), [O III] λ5007 Å (#687) and [S II] λ6716+6731 Å (#702), as well as in broadband Bessel B (#639), V (#641), R(#642), and Gunn *i* (#705). A colour composite of Hen 2-155 made from the narrowband exposures is presented in figure 1, while examples of the individual exposures in each of the narrowband filters (including Hβ-continuum, where the central star is highlighted) are shown in figure 3.

Further images of Hen 2-161 were taken using a Cousins *I*-band filter and the SAAO CCD instrument mounted on the SAAO 1.0-m telescope on the night of April 2nd 2012. The 1 K×1 K STE4 CCD was employed without binning, resulting in a pixel scale of 0.31″×0.31″ pixel^{-1}.

Contamination from high nebular background can make precision photometry of the central star difficult, even leading to spurious variability (often correlated with the seeing; Jones 2011). As such, the choice of filter for monitoring was made based on estimates of the nebular background level with respect to the brightness of the central star in each filter. Previous monitoring campaigns (and surveys) have experienced most success with *I*-band monitoring, as this offers the best combination of broad bandpass (to reduce exposure times) and avoids the brightest nebular emission lines. However, for brighter nebulae with similarly bright central stars (like Hen 2-155), even the

[2] http://starlink.jach.hawaii.edu/

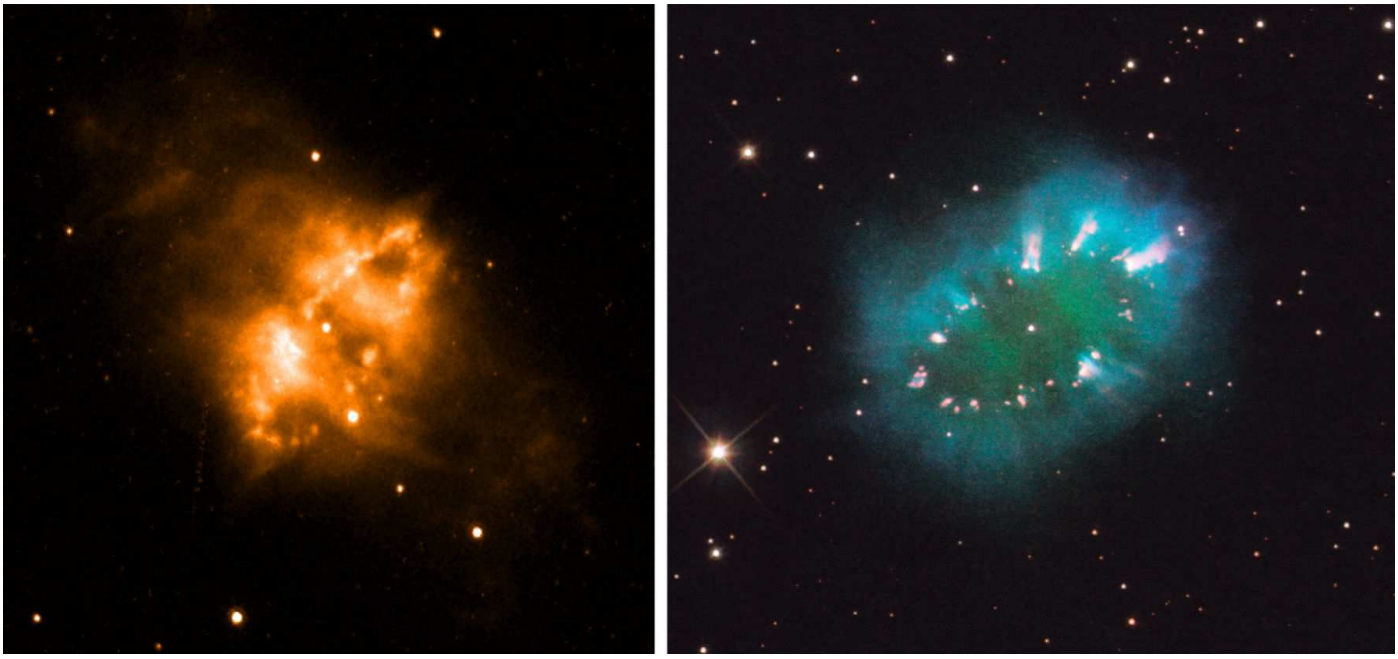

Fig. 2. HST images of Hen 2-161 (left, see also Sahai et al. 2011) and The Necklace (right; Corradi et al. 2011) highlighting their remarkably similar appearances (elongated with knotty waists). The image of Hen 2-161 is in the light of Hα+[N II] λ6584 Å, measuring roughly 20″×20″, while The Necklace image is a colour composite (Credit: NASA, ESA, and the Hubble Heritage Team (STScI/AURA)) measuring roughly 39″×35″. Note the that the central star of Hen 2-161 is offset to the Northeast from the geometric centre of the nebular ring (in both images, North is up and East is to the left).

I-band can show marked nebular emission, in these cases, monitoring can be successfully performed in Hβ-continuum. The Hβ-continuum filter (#743) excludes *all* nebular emission lines reducing the nebular contamination purely to continuum emission, offering the opportunity to observe the central star with minimal influence from the nebula. Given the large aperture of the ESO-NTT and the bright nature of the central star of Hen 2-155, photometric monitoring was possible in Hβ-continuum with high signal-to-noise ratio and with minimal nebular contamination.

Even with the use of filters excluding the majority of the nebular emission, some remains, as such photometry was extracted from both targets with an aperture tailored to a diameter of roughly 3× the maximum seeing during the observations (5″, thus minimising the variable contamination in the aperture; Jones 2011). Photometry was performed using the SExTRACTOR software (Bertin & Arnouts 1996), and the differential magnitude of the central stars measured against non-variable field stars. The *I*-band observations of Hen 2-161 were then placed on an absolute scale using catalogue photometry from DENIS (Epchtein et al. 1999) and the methodology described in Boffin et al. (2012a), with an approximate precision of 0.05 mag (derived from the dispersion of detector zero points calculated from each field star). The Hβ-continuum observations of Hen 2-155 were also placed on an approximate absolute scale using standard stars observed during the observing runs (this can only be considered approximate due to the variable nature of extinction during each night and each run, however as the value of each data point is determined by relative brightness to field stars no spurious variability can have been introduced as part of this process). All photometric measurements and their uncertainties are shown in tables 2 and 3 available in the online version, and in machine-readable format via anonymous FTP from the CDS.

2.2. Spectroscopy

2.2.1. Hen 2-155

The central star of Hen 2-155 was observed on the night of March 19 2013 with FORS2 mounted on the ESO-VLT's Antu telescope (Appenzeller et al. 1998). The instrument set-up consisted of a longslit measuring 0.5″×6.8′, the GRIS_1400V grism and a mosaic of two unbinned 4k×2k MIT/LL CCDs, offering a spectral resolution of roughly 0.7Å with a spectral range of ~4560–5860Å. The observations consisted of 13 contiguous exposures of 900-s followed by a further exposure of 1200-s. The frames were de-biased and flat-fielded in IRAF[3]. We then used PAMELA (Marsh 1989) to remove the sky contribution and obtain the 1D spectra by means of optimal extraction (Horne 1986) as implemented in PAMELA.

The wavelength scale was obtained from one arc spectrum taken during the FORS2 daytime standard calibration routines. We checked for any instrument flexure by monitoring the stability of the nebular [O III] λ4959 emission line. This nebular line was slowly shifting with time, so we removed this trend from each individual spectrum accordingly. This wavelength calibration process and the radial velocity analysis presented below were carried out in MOLLY[4].

The nebula of Hen 2-155 was observed again with the VLT-FORS2 on the night of March 14 2014, with an exposure time of 1200-s employing the GRIS_1200B grism (3660 Å< λ <5110Å), directly followed by a 120-s exposure taken with the GRIS_1200R grism and a GG435 filter (5750 Å< λ <7310Å).

[3] IRAF is distributed by the National Optical Astronomy Observatories.

[4] Tom Marsh's MOLLY package is available at http://deneb.astro.warwick.ac.uk/phsaap/software/molly/html/INDEX.html

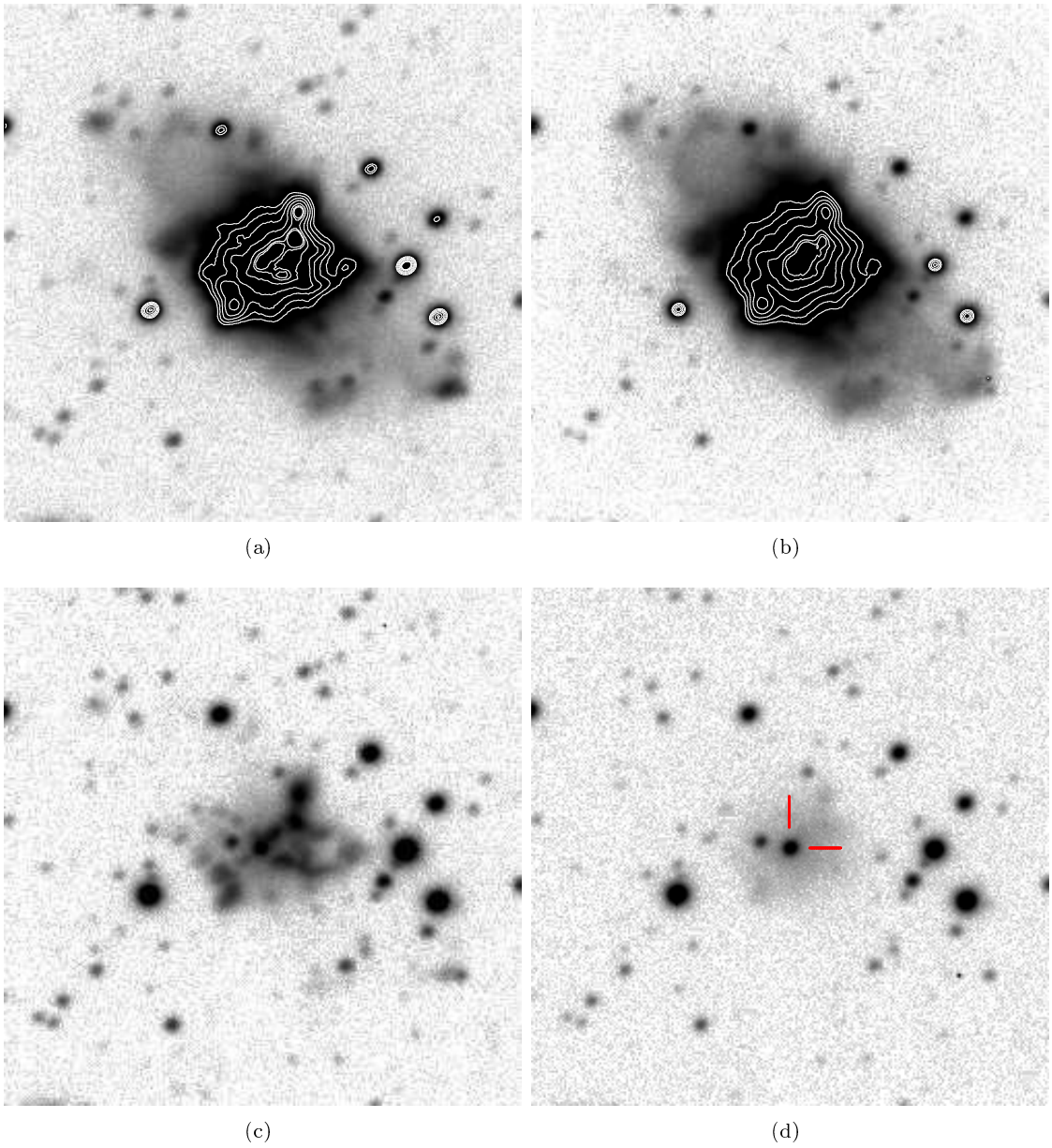

Fig. 3. NTT-EFOSC2 images of Hen 2-155 in the light of (a) Hα+[N II], (b) [O III] λ5007 Å, (c) [S II] λ6716+6731 Å and (d) Hβ-continuum (with central star highlighted). North is up, East to the left and each image measures 1′×1′. All images are displayed on a logarithmic scale. The contours in (a) and (b) represent the 99.7, 99.5, 99, 98, 97, 96 and 95th percentiles and highlight the brighter central structures visible in each filter.

Both spectra were taken using a 0.7″×6.8′ slit (at a position angle of 40 °, along the major axis of the nebula) and binning of 2×2 (providing a resolution of approximately 1.5Å). Standard STARLINK routines were employed to bias subtract, flat field correct, wavelength and flux calibrate the spectra (flux calibration was performed using observations of the standard star LTT4816 taken on the same nights and using the same instrumental setups; Hamuy et al. 1992).

2.2.2. Hen 2-161

The central star of Hen 2-161 was observed on 31 May 2012 with the queue-scheduled Southern African Large Telescope (SALT; Buckley et al. 2006; O'Donoghue et al. 2006). The Robert Stobie Spectrograph (RSS; Burgh et al. 2003; Kobulnicky et al. 2003) was used with the PG1300 grating and 1.5″×8′ slit to obtain a 2150-s exposure covering λ = 4278 – 6360 Å, at a mean resolution of 4.1Å and a reciprocal dispersion of 0.66Å pixel^{-1}. Basic reductions were applied using the PySALT[5] package (Crawford et al. 2010). Cosmic ray events were cleaned using the LACOSMIC package (van Dokkum 2001). Wavelength calibration of the contemporaneous Argon arc lamp exposure was performed using standard IRAF tasks IDENTIFY, REIDENTIFY, FITCOORDS and TRANSFORM by identifying the arc lines in each row and applying a geometric transformation to the data frames. The one dimensional spectrum of the central star was extracted using APALL and no nebular subtraction was made.

VLT-FORS2 observations of Hen 2-161 and its central star were acquired on the night of March 14 2014, with an exposure time of 120-s, employing the GRIS_1200R grism and a GG435 filter , and on April 1 2014, with an exposure time of 1140-s and the GRIS_1200B grism (for further details of the setup see section 2.2.1). All spectra were taken using a 0.7″×6.8′ slit (at a position angle of 45°, chosen to cover the major axis of the nebula). Standard STARLINK routines were employed reduce the spectra just as described in section 2.2.1.

3. Analysis

3.1. Hen 2-155

3.1.1. Lightcurve and radial velocities

A Lomb-Scargle analysis was performed in order to determine the periodicity of the variability displayed by the central star of Hen 2-155 using the PERIOD package of the STARLINK software suite (Dhillon et al. 2001). Fig. 4 shows the data folded on the ephemeris determined by the analysis,

$$\text{min HJD} = 2\,455\,985.7865(\pm0.0001) + 0.148275(\pm0.000008)E$$

where min HJD is Heliocentric Julian Date of the Hβ-continuum lightcurve minimum.

The lightcurve shows smooth sinusoidal variation of peak-to-peak amplitude ∼0.15 mag, with eclipses at phase 0 and 0.5. The primary eclipse (as the secondary passes in front of the primary), at phase 0, is approximately 0.2 mag deep, while the secondary eclipse measures approximately 0.05 mag deep. The "v-shaped" eclipse profiles are typical of grazing eclipses, indicating a moderate orbital inclination (high inclinations would lead to total eclipses which have a "flat-bottomed" profile). Given that at least one of the stars should be a post-AGB remnant (having ejected the PN), then the overall sinusoidal variability is likely to arise from the varying projection of the face of the secondary which is being heated by the hot post-AGB star (known as an "irradiation effect" or "reflection effect"). Given the short period, this variability could also be attributed to one or both stars being close to filling their Roche lobes and, as such, presenting a variable surface area throughout the orbit (known as "ellipsoidal modulation"), this effect is usually associated with rarer, double-degenerate binaries (where both components are post-AGB; Hillwig et al. 2010; Bruch et al. 2001; Santander-García et al. 2015). However, "ellipsoidal modulation" presents two peaks per period with any eclipses occurring at the minima, therefore as the curve shows only one peak per period the origin of the overall variability must originate from the irradiation of the secondary by the primary.

The spectra of Hen 2-155 (Fig. 6) show absorption lines associated with a hot, post-AGB star (e.g. O v λ5114 Å) as well as high-excitation emission lines from the nebula (e.g. [Ar IV] λ4711+4740 Å). The spectra also show emission lines which have previously been identified as typical of an irradiated main-sequence secondary star (C IV λ5801+5812 Å).

Radial velocity measurements, of the primary component of the central star of Hen 2-155, were made via a cross-correlation of the individual O v λ5114 Å absorption profiles in the VLT-FORS2 spectra, and using the average profile as a template. In producing this template, the radial velocities of the O v λ5114 Å line were first measured by fitting Gaussians to the individual profiles. This preliminary radial velocity curve was then fit with a sine function and the measured orbital motion removed from each individual spectrum using this sine fit. Finally, the resulting profiles were averaged in order to obtain the template for cross-correlation. This procedure provides a cross-correlation template with good signal-to-noise ratio and a line width representative of that of the individual profiles. The final measured radial velocities (shown folded in the lower panel of Fig. 4 and listed in the online table 4) agree extremely well with the ephemeris determined from the photometry, clearly showing that the photometric period is also the orbital period. The variation is well fit by a sinusoid of amplitude 59.6±1.5 km s^{-1}, indicating an extremely low orbital eccentricity (as would be expected for such a short period system). The relatively low amplitude (given the short period) of the variability strongly indicates that either: the orbital inclination is low (as the amplitude varies with the sine of the inclination), or, the mass ratio, q, is small (as the amplitude varies with $(1+q)^{-2/3}$). As the lightcurve does show shallow eclipses, it is most likely a combination of the two effects that results in the observed amplitude.

All other lines visible in the spectra, including emission lines which may be associated with the secondary of the system (e.g. N III λ4634+4641 Å and C IV λ5801+5812 Å), were also inspected for radial velocity shifts. All but the C IV complex at ∼5800 Å were found to be non-variable or too weak to be measured (e.g. the possible detection of O VI λ5291 Å). These lines were found to move roughly in phase with the O v absorption (a phase shift of 0.037 is calculated from the fit, shown in figure 5) but with a lower amplitude (∼35 km s^{-1} c.f. ∼60 km s^{-1}). The radial velocities measured from the C IV lines, using the same cross-correlation technique as for the O v λ5114 Å absorption feature (described above), are shown folded on the orbital period, along with a sinusoidal fit, in figure 5 and listed in the online table 5. The lower amplitude appears difficult to reconcile with the measured radial velocities of the O v absorption feature, which must originate from the surface of the primary star. The most likely explanation is that these lines form in the wind of the hot primary and as such trace a region above the WD surface but which has to be restricted to a zone more-or-less between the two stars (as emission from an isotropic wind would present the same radial velocity variability as lines originating from the stellar surface). That the emission is restricted to a relatively small region may be indicative of a "hot spot" on the surface of the primary (Deschamps et al. 2013).

[5] http://pysalt.salt.ac.za

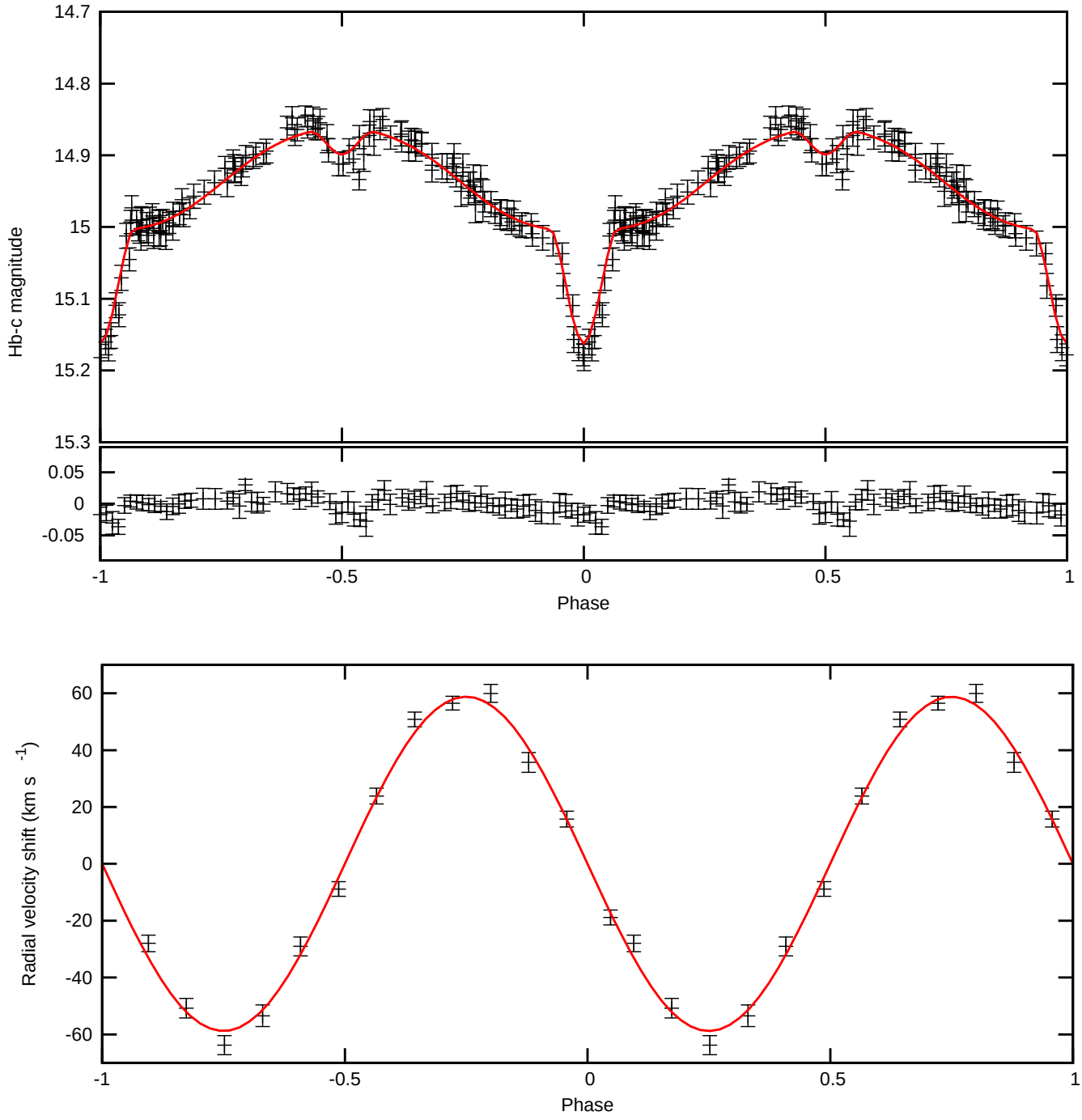

Fig. 4. Folded NTT-EFOSC2 Hβ-continuum photometry of the central star of Hen 2-155 with the NIGHTFALL model overlaid in red (upper panel). Binned residuals between the observed photometry and model are shown in the middle panel. Note that the size of the points represents the photometric uncertainty and contain no estimate of the uncertainty due to variable nebular contamination (which be significant, at certain phases). The lower panel shows the radial velocity measurements of the central star of Hen 2-155 with the predicted radial velocity curve from the NIGHTFALL model overlaid in red.

An unusual profile is found around the He II λ4686 Å nebular emission line (the trailed spectra are shown around this line in figure 7. As is common in spectra of CSPN, the bright nebular emission line is still visible (even after a basic background subtraction, due to its bright and irregular nature) on top of a broad absorption profile moving in phase with the O V absorption line and with a compatible amplitude (we do not measure its amplitude due to the obvious complication of the nebular emission), but at phases of approximately 0.25 and 0.75 there is evidence of high velocity emission in anti-phase with the lines originating from the primary. Given the strong contamination from both the nebula and primary, it is not possible to disentangle this emis-

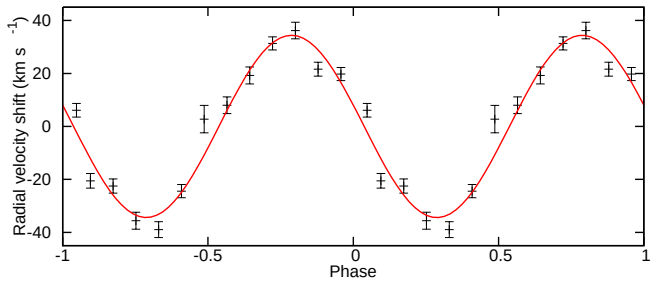

Fig. 5. Radial velocity curve from the C IV lines in Hen 2-155.

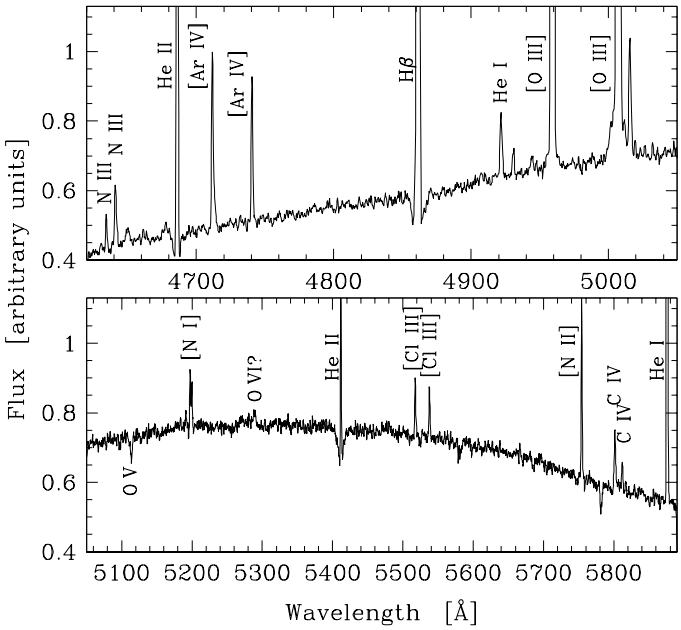

Fig. 6. An example VLT-FORS2 spectrum of Hen 2-155 and its central star.

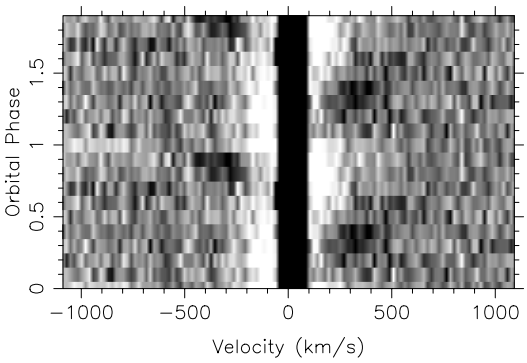

Fig. 7. Trailed spectra showing the emission around the He II λ4686 Å nebular line. Emission is shown in black, and absorption in white.

sion, and therefore determine its origin and possible association with the secondary.

To properly constrain the parameters of the system, simultaneous modelling, of both the radial velocities (from the O V line) and lightcurve, was performed using the NIGHTFALL code[6].

[6] http://www.hs.uni-hamburg.de/DE/Ins/Per/Wichmann/Nightfall.html

Table 6. Modelled and observed binary parameters for Hen 2-155

	Primary	Secondary
$T_{\rm eff}$ (K)	90 000±5 000	3 500±500
Radius ($R_\odot$)	0.31±0.02	0.30±0.03
Log g	–	4.5[a]
Inclination	68.8°±0.8°	
$q = {}^{M_2}/_{M_1}$	$0.21^{+0.05}_{-0.02}$	
M_{tot} ($M_\odot$)	0.75±0.05	
Period (day)	0.148275±0.000008	

Notes. [(a)] A fixed parameter in the modelling

All parameters were varied over a wide range of physical solutions, with the final model being selected for having the lowest χ^2 fit. Detailed reflection was employed in the modelling (with 5 iterations) in order to properly treat the irradiation of the secondary by the primary. A model atmosphere[7] was used for the lower temperature (secondary) component with solar metallicity and log g of 4.5 (Kurucz 1993). The final model lightcurve is shown, along with the residuals to the binned data, in Fig. 4 and the model parameters outlined in Tab. 6.

The model represents an excellent fit, with residuals smaller than the uncertainties of individual observations for almost all data points (the scatter of the radial velocity measurements around the model curve is greater than the photometric data, but still generally a good fit). The modelled progenitor star lies on the stellar evolutionary tracks of both Bloecker (1995, with an He burning remnant) and Vassiliadis & Wood (1994, an H burning remnant with initial mass, M_i=1.0 $M_\odot$, and metallicity, Z=0.001) for a remnant mass of 0.625 $M_\odot$ and 0.623 $M_\odot$, respectively, both in excellent agreement with the modelled mass of 0.62 $M_\odot$ (see figure 8). The post-AGB age is roughly 10 000 years for both of these tracks, which is a reasonable age for a planetary nebula and, for a distance of ~3 kpc (Zhang 1995; Phillips 2004; Stanghellini et al. 2008), would imply an expansion velocity of ~30 km s^{-1} (again, perfectly reasonable for a PN, e.g.; Jones et al. 2010a, 2012). It is worth noting that the model parameters also lie close to tracks from both authors with different parameters (mass, H or He burning, metallicity, etc.), giving an age range from ~3,000 years up to ~25,000 years. Neither end of this expansive range would be out of the question for a PN, however they would imply an exceptionally large or particularly low expansion velocity at the lower and upper age limits, respectively. This range is perhaps reflective of the uncertainty in the starting point for post-AGB tracks, as well as the fact that this is a post-CE system (rather than a single star evolving off the AGB with no external influences, as considered by the models).

The model luminosity (defined by the Boltzmann law, and the model radius and temperature) gives an apparent V_0 for the central star of ~14.7 mag (assuming a reasonable bolometric correction of −7; Reed 1998). From the single i-band observation taken at a phase of 0.67 (we choose not to use the V-band observation due to the extremely high levels of nebula contamination), we measure an extinction-corrected V_0 of ~14.4 mag (uncorrected V_0 of 15.6 mag)[8]. At first this would appear inconsistent, however, noting that the contribution from the secondary

[7] http://kurucz.harvard.edu/grids/gridP00/ip00k2.pck19

[8] Extinction correction performed assuming the extinction law of Howarth (1983), a $c(H\beta)$ of 0.74 (see section 3.1.2), and $(V-I)_O$ = −0.40 (Ciardullo et al. 1999).

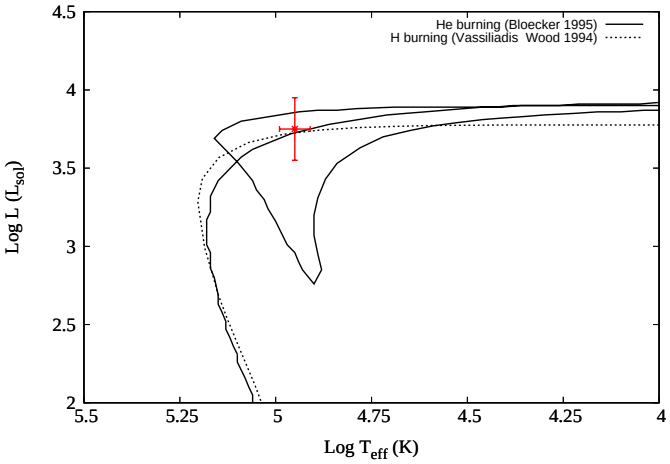

Fig. 8. The temperature and luminosity of the model central star of Hen 2-155 overlaid on top of evolutionary tracks for a remnant of mass 0.625 $M_\odot$ taken from Bloecker (1995) and 0.623 $M_\odot$ taken from Vassiliadis & Wood (1994).

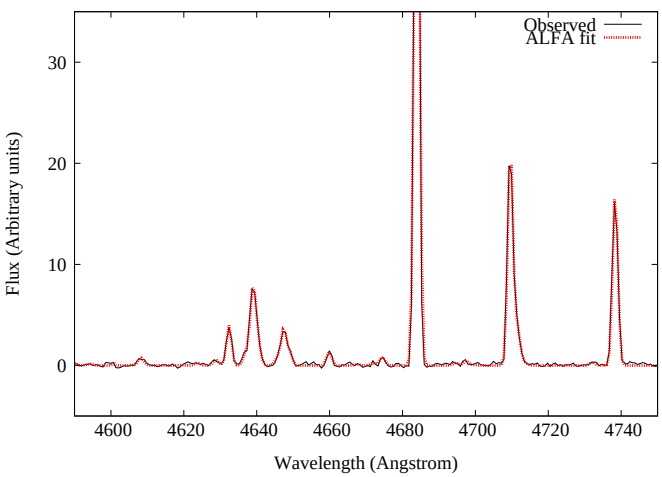

Fig. 9. The continuum-subtracted observations and ALFA fit for a subsection of the FORS2 GRIS_1200B spectrum of the nebula Hen 2-155, covering the C III and N III recombination lines as well as several lines of the V1 O II multiplet, which are critical in determining the nebular *adf*.

is near maximum at this phase, the non-negligible nebular contamination, as well as the uncertainties on the assumed values (particularly the distance), the two values are most certainly consistent and provide a valuable check of the model.

The model temperature of the primary star is, at 90 kK, in relatively poor agreement with those in the literature determined by the Zanstra method (51±10 kK and 73±10 kK for He I and He II Zanstra temperatures, respectively; Kaler & Jacoby 1991). This is to be expected because the Zanstra method depends on accurate measurement of broadband central star magnitudes which will, of course, be contaminated by the contribution from the companion star (as seen in Jones et al. 2014a). Furthermore, the Zanstra temperature determinations assume an optically thick nebula, which would not necessarily be the case for such a hot central star. As such, the Zanstra temperatures can only be considered lower limits for the true central star temperature. The poor agreement between the Zanstra temperatures calculated from Hydrogen and Helium emission lines, further indicates that these temperatures may not be reflective of the true central star temperature. Kaler & Jacoby (1991) found a strong correlation between the intensity of the nebular [O III] λ5007 Å line and the central star temperature, and via their analytical relationship the Stoy Temperature of the central star would be expected to be ~90,000 K, in good agreement with the modelled temperature. Furthermore, the presence of O VI emission, in the VLT-FORS2 spectrum of the central star, indicates a high stellar temperature, probably around ~100,000 K (much higher than this and the O V lines become much less pronounced, lower and the O VI line would not be present).

The modelled secondary mass and temperature of 0.13 $M_\odot$ and 3 500 K are in rough agreement with those predicted by ZAMS models for an M5V star (the ZAMS temperature of a 0.13 $M_\odot$ star with solar metallicity is approximately 3 000 K; Paxton et al. 2011), here the slightly elevated temperature could be partly due to the uncertainty on the model temperature as well as the fact that the high levels of irradiation from the primary may cause a global increase in temperature rather than just an increase on the "day side" of the secondary. The modelled radius, however, is much greater than expected for a main sequence star of this mass (almost a factor of two larger, more in keeping with a star of mass 0.3 $M_\odot$). This "inflation" could be associated with the high levels of irradiation from the primary, but could also be a symptom of mass transfer just before entering the CE phase. Further discussion of this "inflation" shall be reserved for Section 4.

The orbital plane, at an inclination of 68.8°±0.8°, is expected to be perpendicular to the nebular symmetry axis (Jones et al. 2014b; Nordhaus & Blackman 2006), while the nebula appears to be viewed more or less side-on (implying an inclination of ~90° for the binary orbital plane). However, it is not possible to determine the nebular orientation without detailed spatio-kinematic modelling (which necessitates the acquisition of high-resolution, spatially-resolved, nebular spectroscopy) and, moreover, PNe with similar projections have been found to have inclinations that would be generally consistent with the modelled inclination (for example, HaTr 4 appears similarly side-on but, in fact, has an inclination of ~75°; Tyndall et al. 2012).

3.1.2. Ionic and total abundances of Hen 2-155

Apertures containing nebular emission from Hen 2-155 were extracted from the VLT-FORS2 spectroscopy described in section 2. From the resulting one-dimensional spectra, emission line fluxes were derived using the ALFA code (Wesson, in prep.; Jones et al. in prep.), which optimises the parameters of Gaussian fits to the line profiles using a genetic algorithm, fitting all lines simultaneously after subtracting a globally-fitted continuum (see figure 9 for a demonstration of the quality of the fit provided by ALFA). These emission line fluxes were then used to derive abundances using the NEAT code (Wesson et al. 2012). This code corrects for interstellar extinction using measured Balmer line ratios, and then determines temperatures and densities from the standard diagnostics. Elemental abundances are then calculated as the flux-weighted averages of the emission lines from each species, and total chemical abundances using the ionisation correction scheme of Delgado-Inglada et al. (2014). At each stage, uncertainties are robustly propagated using a monte carlo technique.

Measured and dereddened fluxes (along with their 1σ uncertainties) for Hen 2-155 are shown in Table 6, while the determined nebular properties are listed in table 8. The reddening

Table 8. Extinction, temperatures, and densities as determined by the empirical analysis using the NEAT code.

	Hen 2-155	Hen 2-161
$c(H_\beta)$	0.74± 0.01	1.21±0.01
T_e([N II]) (K)	–	9800±360
T_e([O III]) (K)	11660±40	8190±110
n_e([O II]) (cm^{-3})	1300±70	1870±110
n_e([S II]) (cm^{-3})	1390±55	1500±89
n_e([Ar IV]) (cm^{-3})	670±160	–

Table 9. Ionic abundances, relative to Hydrogen (in the form $\frac{ion}{H}$), as determined by the empirical analysis using the NEAT code. All abudances are calculated using CELs unless otherwise indicated.

Ion	Hen 2-155	Hen 2-161
C^{2+} (ORLs)	$3.39 \times 10^{-4}{}^{+1.9\times10^{-5}}_{-1.8\times10^{-5}}$	$2.13 \times 10^{-3}{}^{+4.4\times10^{-5}}_{-4.3\times10^{-5}}$
C^{3+} (ORLs)	$1.51 \times 10^{-4}{}^{+1.7\times10^{-5}}_{-1.6\times10^{-5}}$	$2.75 \times 10^{-3}{}^{+3.4\times10^{-4}}_{-3.4\times10^{-4}}$
N^{+}	$5.27 \times 10^{-6}{}^{+1.8\times10^{-8}}_{-1.7\times10^{-8}}$	$7.89 \times 10^{-6}{}^{+8.1\times10^{-7}}_{-7.3\times10^{-7}}$
O^{+}	$1.22 \times 10^{-5}{}^{+1.2\times10^{-7}}_{-1.2\times10^{-7}}$	$1.52 \times 10^{-5}{}^{+2.7\times10^{-6}}_{-2.3\times10^{-6}}$
O^{2+} (CELs)	$1.43 \times 10^{-4}{}^{+2.9\times10^{-6}}_{-2.8\times10^{-6}}$	$2.05 \times 10^{-4}{}^{+1.2\times10^{-5}}_{-1.1\times10^{-5}}$
O^{2+} (ORLs)	$9.01 \times 10^{-4}{}^{+3.8\times10^{-5}}_{-3.6\times10^{-5}}$	$2.26 \times 10^{-3}{}^{+8.5\times10^{-5}}_{-8.2\times10^{-5}}$
adf(O^{2+})	6.3	11.0
Ne^{2+}	$5.07 \times 10^{-5}{}^{+6.7\times10^{-7}}_{-6.6\times10^{-7}}$	$7.75 \times 10^{-5}{}^{+5.2\times10^{-6}}_{-4.9\times10^{-6}}$
Ar^{2+}	$8.76 \times 10^{-7}{}^{+4.7\times10^{-8}}_{-4.5\times10^{-8}}$	$1.66 \times 10^{-6}{}^{+6.5\times10^{-8}}_{-6.2\times10^{-8}}$
Ar^{3+}	$3.91 \times 10^{-7}{}^{+5.6\times10^{-9}}_{-5.5\times10^{-9}}$	$1.87 \times 10^{-7}{}^{+2.4\times10^{-8}}_{-2.2\times10^{-8}}$
S^{+}	$2.44 \times 10^{-7}{}^{+2.0\times10^{-9}}_{-2.0\times10^{-9}}$	$2.76 \times 10^{-7}{}^{+2.6\times10^{-8}}_{-2.4\times10^{-8}}$
S^{2+}	$1.83 \times 10^{-6}{}^{+5.7\times10^{-8}}_{-5.6\times10^{-8}}$	$2.50 \times 10^{-6}{}^{+3.4\times10^{-7}}_{-3.0\times10^{-7}}$

is found to be $c(H_\beta)$=0.74±0.01 in relatively good agreement with the values found in the literature (0.81, Cavichia et al. 2010; 0.98–1.01, Cahn et al. 1992), as are the individual line fluxes c.f. those presented by Cavichia et al. (2010).

The final ionic and total abundances for Hen 2-155 are shown in tables 9 and 10, respectively. The abundances indicate that Hen 2-155 is a non-type I PNe (based on the He/H and N/O ratios; Peimbert 1978; Kingsburgh & Barlow 1994). Furthermore, comparison of Oxygen abundances determined from collisionally excited lines (CELs) and optical recombination lines (ORLs), show a strong discrepancy – known as an abundance discrepancy factor (*adf*) – whereby the abundance from ORLs is a factor of 6 greater than that from CELs. Such discrepancies are well known, appearing in analyses of all photoionised nebulae, but are generally found to be only a factor of a few (1.5–3 in H II regions, while only ~20% of PNe are found to have *adfs* > 5; García-Rojas & Esteban 2007; Wesson et al. 2005). Further discussion of this enhanced *adf* is reserved for section 4.

3.1.3. Photoionisation modelling of Hen 2-155

In order to confirm that a hot (T~90 kK) central star, predicted by our modelling of the photometric light curve, is consistent with the overall ionisation state of the nebula, we constructed a simple photoionisation model for comparison to our measured emission line fluxes. It is important to note that our model is only intended to show that the ionisation state of the nebula is consistent with the central star temperature determined from the simultaneous modelling of light- and radial velocity curves. It is not intended to provide a realistic description of the nebula, given that the nebula is clearly both irregular and filamentary (Fig. 3) and that we have no information about surface abundances in the central star with which to realistically estimate the ionising spectrum.

Table 10. Total nebular abundances from Hen 2-155 and Hen 2-161, determined using the NEAT code.

Element	Hen 2-155	Hen 2-161
H	1.00	1.00
He	$0.11^{+6.5\times10^{-4}}_{-6.5\times10^{-4}}$	$0.13^{+7.7\times10^{-4}}_{-8.3\times10^{-4}}$
C (ORLs)	$4.91 \times 10^{-4}{}^{+2.5\times10^{-5}}_{-2.4\times10^{-5}}$	$4.87 \times 10^{-3}{}^{+3.5\times10^{-4}}_{-3.3\times10^{-4}}$
N	$7.01 \times 10^{-5}{}^{+1.5\times10^{-6}}_{-1.4\times10^{-6}}$	$1.14 \times 10^{-4}{}^{+8.9\times10^{-6}}_{-8.2\times10^{-6}}$
O	$1.62 \times 10^{-4}{}^{+3.0\times10^{-6}}_{-2.9\times10^{-6}}$	$2.21 \times 10^{-4}{}^{+1.2\times10^{-5}}_{-1.1\times10^{-5}}$
Ne	$5.74 \times 10^{-5}{}^{+6.7\times10^{-7}}_{-6.6\times10^{-7}}$	$8.35 \times 10^{-5}{}^{+5.4\times10^{-6}}_{-5.1\times10^{-6}}$
S	$3.50 \times 10^{-6}{}^{+1.1\times10^{-7}}_{-1\times10^{-7}}$	$4.81 \times 10^{-6}{}^{+6.7\times10^{-7}}_{-5.9\times10^{-7}}$
Ar	$1.26 \times 10^{-6}{}^{+4.8\times10^{-8}}_{-4.6\times10^{-8}}$	$1.84 \times 10^{-6}{}^{+7.8\times10^{-8}}_{-7.5\times10^{-8}}$

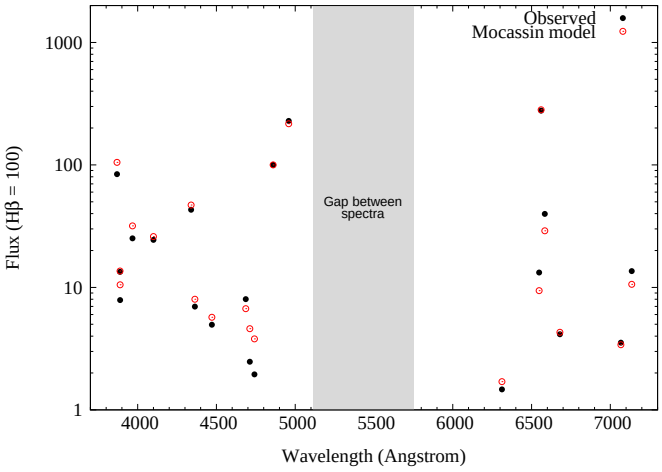

Fig. 10. A comparison of emission line fluxes from the MOCASSIN model of Hen 2-155 and those measured from the FORS2 spectroscopy (Table 6).

We modelled the nebula, using MOCCASIN (Ercolano et al. 2003), as a sphere of radius 10^{18} cm, estimated from the angular extent of the nebula and a distance of 3 kpc. The model has uniform hydrogen density of 1000 cm^{-3} (see previous section), and abundances based on the empirical analysis of observed line fluxes (for a list of the final abundances used see table 10). The model reproduces fairly well the overall emission spectrum of the nebula (see figure 10) despite being so simplistic. The central star in the model is a blackbody with a temperature of 90 kK and a luminosity of 5200 $L_\odot$, both matching well with the temperature and luminosity determined from simultaneous modelling of the light- and radial velocity curves. A more realistic spectral shape for the ionising source (i.e. not a perfect blackbody) and more realistic density distribution would certainly affect the ionisation balance, but the model clearly shows that a hot central star is consistent with the measured emission line ratios. As such, we conclude that the temperature determined in this work, 90 kK, constitutes a more accurate estimate of central star temperature than those made using other methodologies in the literature (e.g. Zanstra temperatures).

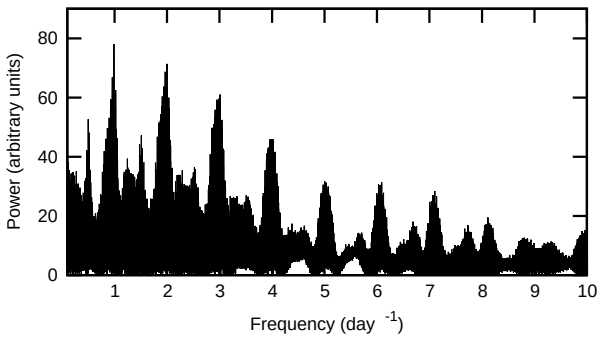

Fig. 11. Lomb-Scargle periodogram of the photometric observations of Hen 2-161.

3.2. Hen 2-161

3.2.1. Stellar photometry and spectroscopy

The photometric observations of Hen 2-161 were taken in two different filters - the majority in Gunn-*i* taken using NTT-EFOSC2 with the rest taken in Cousins-*I* with the SAAO CCD mounted on the SAAO 1.0-m. In order to ensure no colour effects were present in the combination of data taken through two different *I*-band filters, the relative magnitude of several field stars (used in photometering the central star) were measured, with the results generally agreeing within the uncertainties of the individual measurements. As such, we do not apply any colour correction to the photometry of the central star - this may, indeed, induce spurious variability, so the results will be assessed in the context of the combined data and the NTT data alone (as the vast majority of the data originate from this telescope).

A Lomb-Scargle analysis was performed for the complete photometry of the central star of Hen 2-161 using the PERIOD package of the STARLINK software suite (Dhillon et al. 2001). The data show clear variability, but unfortunately any true period remains difficult to ascertain most likely due to it being extremely close to the periodic aliases of nightly observing (12 hours and 1 day). The Lomb-Scargle periodogram of the data is presented in figure 11, highlighting the strength of each of the peaks around each alias. The data show a maximum variation of roughly 0.2 mag (0.15 mag excluding the SAAO 1.0-m data), although, given the possible periods, this is not certain to be the true peak-to-peak amplitude of the variability. It is highly unlikely that this variability is spurious, given that it does not correlate with any aspect of the observing parameters other than the time of the observation (spurious variability due to nebular contamination or colour effects generally can be found to correlate with the seeing or airmass at the time of the observation; Jones 2011). Even if the inclusion of the SAAO 1.0-m data is erroneous, there is still a clear upward trend in the data obtained with EFOSC2-NTT (see figure 12).

The VLT-FORS2 spectra and SALT-RSS spectrum all show absorption features associated with a hot post-AGB nebular progenitor (e.g. He II λ4542 Å, He II λ5412 Å, N V λ4604 Å) as well as emission lines frequently, but not exclusively (see above discussion of these lines in the spectra of Hen 2-155), associated with irradiated, main-sequence companions (see figure 13, and Miszalski et al. 2011b; Corradi et al. 2011). Both absorption and emission features visible in all spectra were inspected for velocity shifts, with respect to nebular emission lines (e.g. Hβ,

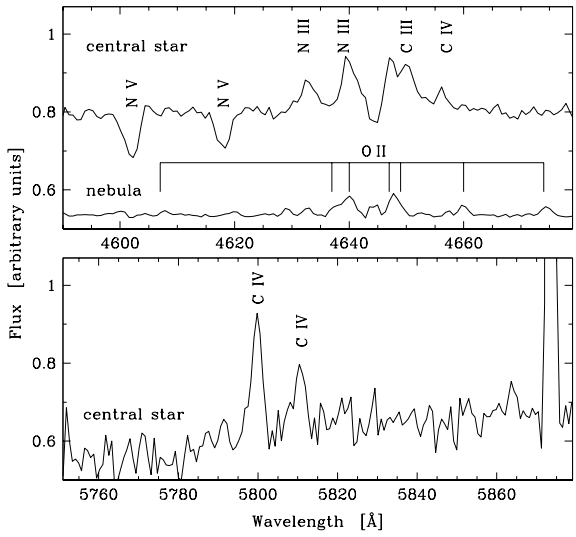

Fig. 13. VLT-FORS2 spectroscopy of the central star of Hen 2-161 displaying both absorption features from a hot post-AGB central star and emission line complexes frequently associated with an irradiated, main-sequence secondary. In both panels, the central star spectrum is shown without any nebula subtraction. In the upper panel, an extraction of the nebula close to the central star is displayed (with an arbitrary offset) in order to highlight that the emission lines originate from the central star and not from the nebula.

He I λ4472 Å, [O III] λ4959 Å), with all radial velocities agreeing within the uncertainties of the measurements (which, given the low resolution of the spectrum, are rather large for this purpose). This is, perhaps, not unreasonable given that, for a period of ∼1 day, the spectra would have all taken at around the same phase which may have been close to conjunction where any radial velocity shifts would be minimal (this is consistent with the phases of the highly speculative sine curve overlaid in fig 12 where all spectra would have been taken at phase ∼0). However, this does mean that we cannot rule out that the variability of the central star is not associated with binarity, but, given the persistent nature of the observed photometric variability (pulsations often vary on timescales shorter than the 2 years over which our observations span, particularly in such a young post-AGB object; Winget & Kepler 2008), the presence of emission lines associated with an irradiated secondary, and the off-centre central star (often associated with central star binary; Soker & Rappaport 2001; Jones et al. 2010b), we conclude that Hen 2-161 is most likely host to a close binary central star with a possible orbital period of approximately 1 day. We strongly encourage follow-up observations, particularly at other longitudes, in order to confirm and further constrain its nature as a post-CE binary.

3.2.2. Ionic and total abundances of Hen 2-161

Just as for Hen 2-155 (Section 3.1.2), nebular apertures of Hen 2-161 were extracted from the VLT-FORS2 spectroscopy described in section 2 and processed using the ALFA and NEAT codes. The measured and dereddened fluxes (along with their

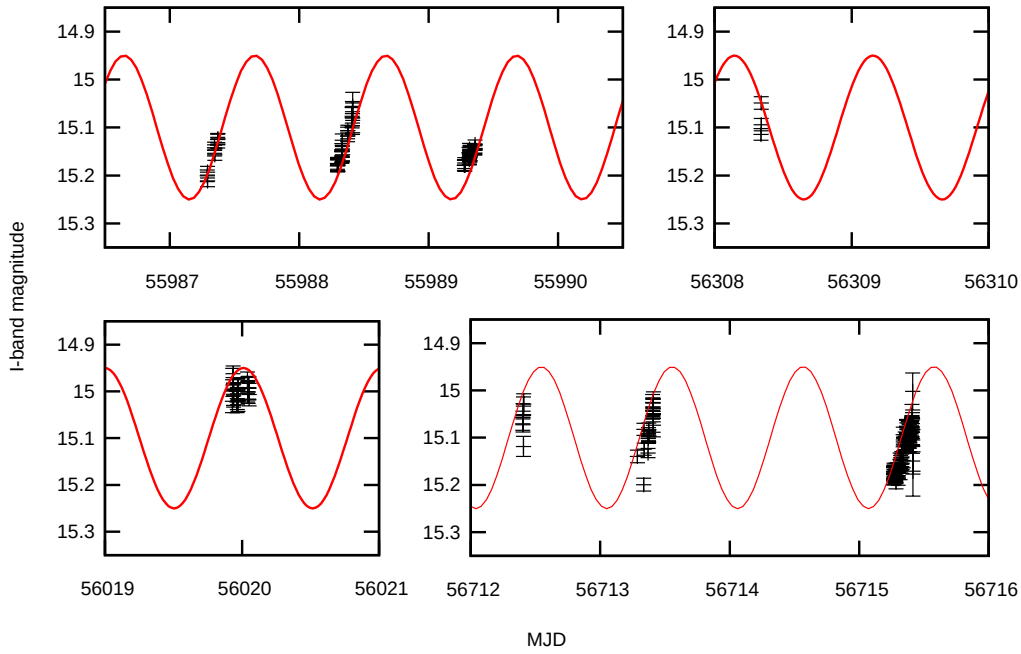

Fig. 12. *I*-band photometry of the central star of Hen 2-161 with an overlaid sinusoid of period 1.011 day (the peak of the periodogram shown in figure 11). The observations from the SAAO 1.0-m telescope (taken in a different *I*-band filter to the rest of the observations) are shown in the lower left panel, highlighting that even without adding the data from this telescope, the variability is still clear. The scatter in the points may be due to an error in the period or to variable nebula contamination as seen in Miszalski et al. (2011b).

1σ uncertainties) for Hen 2-161 are shown in Table 6, while the determined properties of the nebula are listed in table 8. The reddening is found to be $c(\mathrm{H}_\beta)$=1.21±0.01, while the literature values range from 0.35–1.80 (Cahn et al. 1992), depending on the method used in its determination (the upper value is determined from the ratio of radio 5 GHz flux density and Hβ, while the lower is from the ratio of Hα and Hβ). Given that our measurement is the weighted average of all the Balmer line ratios available in the covered wavelength range (which covers Hα through to Hζ), and the results are consistent across all ratios (as reflected by the relatively small uncertainty), it is clear that the value measured here must represent the most accurate determination of the reddening to date.

The final ionic and total abundances are shown in tables 9 and 10, respectively. Hen 2-161 shows systematically higher heavy element abundances than Hen 2-155, just about satisfying the general criterion for Type I PNe (He/H≥0.125, N/O≥0.5 Peimbert 1978)[9]. This may be indicative of a higher mass progenitor or that the binary evolution has had little (or lessened) effect on the chemical evolution of the primary (De Marco 2009). However, just as for Hen 2-155, Hen 2-161 displays a large *adf* (over 10), possibly typical of central star binarity (see section 4).

4. Discussion

The central star of Hen 2-155 is a photometrically variable binary star with a period of 0.148 day, while the central star of Hen 2-161 has also been shown to be photometrically variable with a possible period of ∼1 day. While a ∼1 day period is highly suspicious, one other bCSPN is known to have a period extremely close to ∼1 day (Abell 65, Shimansky et al. 2009; Bond & Livio 1990) meaning that such a period should not be ruled out. However, it is ultimately unclear whether the photometric variability in the central star of Hen 2-161 is associated with binarity, but we conclude that it is the most likely cause and encourage follow-up observations (both photometric and spectroscopic) at in order to fully reconstruct any orbit. Given its brightness (I ∼15.1 mag) and southern declination, it should be easily accessible with available telescopes, the main constraint comes in the form of seeing as, due to a bright star approximately 2″ away from the CSPN (to the South, more or less on the edge of the nebular ring, see figure 2), good seeing is needed to ensure photometry of the central star alone.

The central star of Hen 2-155 was also found to be a single-lined, radial-velocity variable with a period and ephemeris consistent with that derived from the photometric observations. Simultaneous modelling of the lightcurve and radial velocity curve shows that the system consists of a hot nebular progenitor, with a temperature of ∼90 kK, and a much cooler companion. The modelled primary mass, radius and temperature are consistent with evolutionary tracks and the ionisation state of the nebula. The modelled secondary has a much larger radius, and slightly higher temperature, than expected for its mass. It is worthy of note, that there is an indication of emission from the secondary star in the system, but that its radial velocity in this line could not be measured due to low signal-to-noise and contamination from spectral features of the primary and nebula.

Radial velocity measurements of the C IV λ5801+5812 Å emission lines present in the spectra of Hen 2-155 show variability in phase with that of the O V absorption lines originating

[9] Note that Kingsburgh & Barlow (1994) proposed a higher threshold for being Type I which Hen 2-161 does not satisfy (N/O≥0.8)

Table 11. Binary CSPNe from the literature where parameters for both primary and secondary stars have been derived from simultaneous modelling of photometric and radial velocity observations. The upper five have main-sequence companions, while the lower two are shown to be double-degenerates.

Nebula	Period (day)	M_{CS} ($M_\odot$)	R_{CS} ($R_\odot$)	T_{CS} (kK)	M_S ($M_\odot$)	R_S ($R_\odot$)	T_S (kK)	Notes
Abell 46[a]	0.47	0.51±0.05	0.15±0.02	49.5±4.5	0.15±0.02	0.46±0.02	3.9±0.4	Double-lined
Abell 63[a]	0.47	0.63±0.05	0.35±0.01	78±3	0.29±0.03	0.56±0.02	6.1±0.2	Double-lined
Abell 65[b]	1.00	0.56±0.04	0.056±0.008	110±10	0.22±0.04	0.41±0.05	5.0±1.0	Not eclipsing
BE Uma[c]	2.29	0.70±0.07	0.08±0.01	105±5	0.36±0.07	0.72±0.05	5.8±0.3	Double-lined
Ds 1[d]	0.36	0.63±0.03	0.16±0.01	77±3	0.23±0.01	0.40±0.01	3.4±1	Not eclipsing, double-lined
Hen 2-428[e]	0.18	0.88±0.13	0.68±0.04	32.4±5.2	0.88±0.13	0.68±0.04	30.9±5.2	Double-lined
NGC 6026[f]	0.53	0.57±0.05	1.06 ±0.05	38±3	0.57±0.05	0.05±0.01	146±15	-

References. (a) Afşar & Ibanoğlu (2008); (b) Hillwig et al. (2015); (c) Ferguson et al. (1999); (d) Hilditch et al. (1996); (e) Santander-García et al. (2015); (f) Hillwig et al. (2010).

from the primary, but with a lower amplitude. The true origin of this emission is quite uncertain, but it is most likely to originate from the wind of the hot primary and hence trace a region above its surface. It's restriction to a region between the two stars may be associated with a "hot spot" on the surface of the primary from which the wind is enhanced (Deschamps et al. 2013). A "hot spot" would be in keeping with the Roche-lobe filling nature of the secondary, whereby direct impact of mass transferred from the secondary onto the surface of the primary would be responsible for its formation (no accretion disk would be formed because the primary is larger than the circularisation radius for any material transferred onto it). Given the faintness of these lines, and that no other lines display the same behaviour, we conclude that while of great interest and warranting further investigation, this unusual line profile gives no reason to doubt the stellar parameters derived from the modelling.

Only a handful of other binary CSPNe have had their parameters derived by in-depth studies similar to the one presented here [10] (with the results summarised in table 11). Of those seven systems, two are found to be double-degenerates where both stars have evolved to the post-AGB phase, while the other five are found to have secondaries which are greatly inflated with respect to the ZAMS radii for their given masses.

The origin of the inflation seen in the secondaries of CSPNe is unclear, but several possibilities have been considered in the literature. Afşar & Ibanoğlu (2008) considered that the inflated secondaries in Abell 46 and Abell 63 may originate from magnetic activity, ruling this possibility out due to the also increased temperatures (magnetic activity has been shown to result in increased radii and reduced temperatures). de Marco et al. (2008) state that the extreme heating of the secondaries by the much hotter primaries could lead to them "puffing up" as the star is irradiated by leakage of radiation from the "day side" to the "night side", the level of this effect is, however, unclear and may not contribute sufficiently to increase the radii by the levels seen. This hypothesis is, however, supported by the elevated temperatures determined both from the modelling and from spectroscopic observations of the "night side" of the secondaries (de Marco et al. 2008). Finally, the inflation could be associated with mass from the primary being accreted just prior to or during the CE phase, knocking the secondary out of thermal equilibrium. For fully convective secondaries (or those with deep convective envelopes), the amount of matter required to be accreted in order to produce the observed inflation is minimal, but the accretion rate does need to be significant ($\gtrsim 10^{-5}$ $M_\odot\,yr^{-1}$; Prialnik & Livio 1985). Hydrodynamic models indicate that the spiral-in speeds during the CE are highly supersonic, leading to the formation of a bow shock and preventing any material from being accreted by the secondary during the CE phase (Sandquist et al. 1998). However, recently it has been suggested that there could be a period of pre-CE mass transfer which, due to the extremely short nature of the CE, could be responsible for the secondaries being out of thermal equilibrium even after exiting the CE.

The central star of The Necklace is a post-CE binary where the secondary shows clear evidence of being chemically polluted by AGB material from the primary (Miszalski et al. 2013; Boffin 2014a), proving that mass transfer can and does occur in these systems (and possibly in significant quantities - 0.03–0.35 $M_\odot$ in the case of The Necklace). This mass transfer almost certainly occurred immediately prior to the CE, also being responsible for forming the polar jets seen in the nebula (the dynamical ages of the jets are older than that of the central regions of the nebula, which is expected to be the remnant of the ejected CE, Corradi et al. 2011). Interestingly, amongst the other nebulae shown to play host to inflated secondaries, there is a second case where the polar regions of the nebula appear to have been ejected prior to the CE (Abell 63, Mitchell et al. 2007). Estimates of the mass transfer rate during the formation of the jets in these objects are of order 10^{-5}–10^{-4} $M_\odot\,yr^{-1}$ (Tocknell et al. 2014), almost certainly sufficient to produce the inflation found in the secondaries. It is worth noting that, while the other nebulae found to host inflated secondaries, including Hen 2-155, they have yet to be shown to present evidence of polar outflows formed prior to the CE phase. This may just be due to a lack of detailed morpho-kinematical study[11] or simply because these outflows are generally extremely light and may since

[10] Note that other systems have also been subjected to simultaneous modelling of spectroscopic and photometric observations but, due to their non-eclipsing nature (and the lack of multi-band photometry), their parameters (especially radii) could not be derived (e.g. HFG 1; Exter et al. 2005). Similarly, other systems have been modelled based on photometry alone, but here masses can only be estimated via indirect means (e.g. Hen 2-11; Jones et al. 2014a). It is also worth noting that the majority of the other systems listed in table 11 are double-lined spectroscopic binaries, meaning that a more direct constraint can be placed on their mass ratios than in the case of a single-lined binary (as is the case for Hen 2-155, where the parameter is constrained by the modelling).

[11] This may likely be the case for Hen 2-155 given the presence of pairs geometrically opposed knots. Further kinematical study will be essential not only in constraining the morphology of Hen 2-155 but also the nature of these "jet" candidates.

have simply dissipated into the surroundings and are no longer visible.

In this study, both Hen 2-155 and Hen 2-161 are found to display sub-solar, non-type I abundances (Hen 2-161 could be considered a marginal Type I) and higher than average *adfs*, both of which have possible links to binarity. Non-type I abundances can arise naturally from low-mass single star progenitors or high mass progenitors where a binary interaction has cut short the chemical evolution of the progenitor (De Marco 2009) - given that both nebulae display type I-like morphologies, this may be an indication that the latter scenario has played a role (however, this cannot be confirmed with the current observations). Perhaps a stronger link to binarity is the high *adf*, where recent work has shown that the PNe with the highest known *adfs* all host a central binary star (Corradi et al. 2015, Jones et al. in prep; and references therein). High *adfs* also strengthen the link between PNe with binary central stars and other binary phenomena, such as novae, which are also known to display extremely high *adfs* (Wesson et al. 2003, 2008).

We strongly encourage the detailed study of other post-CE CSPN and their host nebulae (as well as the continued search for new systems) in order to improve the statistics and to establish the parameters space for future modelling and study of the CE and its effect on PN formation and evolution. In the immediate future, this work should focus on radial velocity studies and modelling of eclipsing systems for which high-quality photometric monitoring has already been performed (e.g. M3 16, H 2-29 and M 2-19; Miszalski et al. 2008), as eclipsing systems offer the best prospect for well-constrained parameters. For non-eclipsing systems, the greatest uncertainty often arises from the a wide-range of inclinations offering reasonable fits to the data - in this cases, the now well established link between nebular inclination and binary inclination may be used to successfully break the degeneracy. This, however, requires detailed spatio-kinematical modelling of the host nebulae (e.g. Tyndall et al. 2012; Huckvale et al. 2013) in order to determine the inclination of the nebular symmetry axis which can then be assumed to be roughly perpendicular to binary orbital plane (Jones et al. 2012, 2014b; Nordhaus & Blackman 2006).

Acknowledgements. We would like to thank Klaus Werner for his assistance in the interpretation of the stellar spectroscopy, and Tom Marsh for the use of his MOLLY and PAMELA software packages. DJ would like to thank Jorge García-Rojas for useful discussions regarding the interpretation of the nebular spectroscopy.

This paper is based on observations made with ESO Telescopes at the La Silla Paranal Observatory under programme IDs 088.D-0573, 090.D-0435, 091.D-0475, 092.D-0449 & 093.D-0038. This paper includes observations made with the Southern African Large Telescope (SALT) under programme 2012-1-RSA-009, and with the 1m telescope of the South African Astronomical Observatory (SAAO). Based on observations made with the NASA/ESA Hubble Space Telescope, and obtained from the Hubble Legacy Archive, which is a collaboration between the Space Telescope Science Institute (STScI/NASA), the Space Telescope European Coordinating Facility (ST-ECF/ESA) and the Canadian Astronomy Data Centre (CADC/NRC/CSA). This research made use of NASA's Astrophysics Data System; the SIMBAD database, operated at CDS, Strasbourg, France; the VizieR catalogue access tool, CDS, Strasbourg, France.

This research has been supported by the Spanish Ministry of Economy and Competitiveness (MINECO) under grants AYA2012–38700 and AYA2012-35330. PRG acknowledges support from the MINECO under the Ramón y Cajal programme (RYC–2010–05762).

Finally, we wish to thank the anonymous referee for their comments which have improved the detail of this manuscript.

References

Afşar, M. & Ibanoğlu, C. 2008, MNRAS, 391, 802
Appenzeller, I., Fricke, K., Fürtig, W., et al. 1998, The Messenger, 94, 1
Bertin, E. & Arnouts, S. 1996, A&AS, 117, 393
Bloecker, T. 1995, A&A, 299, 755
Boffin, H. M. J. 2014a, in Ecology of Blue Straggler Stars
Boffin, H. M. J. 2014b, in ASP proceedings of the "19th European White Dwarf Workshop"
Boffin, H. M. J., Miszalski, B., & Jones, D. 2012a, A&A, 545, A146
Boffin, H. M. J., Miszalski, B., Rauch, T., et al. 2012b, Science, 338, 773
Bond, H. E. 2000, in Astronomical Society of the Pacific Conference Series, Vol. 199, Asymmetrical Planetary Nebulae II: From Origins to Microstructures, ed. J. H. Kastner, N. Soker, & S. Rappaport, 115
Bond, H. E. & Livio, M. 1990, ApJ, 335, 568
Bruch, A., Vaz, L. P. R., & Diaz, M. P. 2001, A&A, 377, 898
Buckley, D. A. H., Swart, G. P., & Meiring, J. G. 2006, in Society of Photo-Optical Instrumentation Engineers (SPIE) Conference Series, Vol. 6267, Society of Photo-Optical Instrumentation Engineers (SPIE) Conference Series, 0
Burgh, E. B., Nordsieck, K. H., Kobulnicky, H. A., et al. 2003, in Society of Photo-Optical Instrumentation Engineers (SPIE) Conference Series, Vol. 4841, Society of Photo-Optical Instrumentation Engineers (SPIE) Conference Series, ed. M. Iye & A. F. M. Moorwood, 1463–1471
Buzzoni, B., Delabre, B., Dekker, H., et al. 1984, The Messenger, 38, 9
Cahn, J. H., Kaler, J. B., & Stanghellini, L. 1992, A&AS, 94, 399
Cavichia, O., Costa, R. D. D., & Maciel, W. J. 2010, RevMexAA, 46, 159
Ciardullo, R., Bond, H. E., Sipior, M. S., et al. 1999, AJ, 118, 488
Corradi, R. L. M., García-Rojas, J., Jones, D., & Rodríguez-Gil, P. 2015, ApJ, 803, 99
Corradi, R. L. M., Sabin, L., Miszalski, B., et al. 2011, MNRAS, 410, 1349
Crawford, S. M., Still, M., Schellart, P., et al. 2010, in Society of Photo-Optical Instrumentation Engineers (SPIE) Conference Series, Vol. 7737, Society of Photo-Optical Instrumentation Engineers (SPIE) Conference Series
De Marco, O. 2009, PASP, 121, 316
de Marco, O., Hillwig, T. C., & Smith, A. J. 2008, AJ, 136, 323
Delgado-Inglada, G., Morisset, C., & Stasińska, G. 2014, MNRAS, 440, 536
Deschamps, R., Siess, L., Davis, P. J., & Jorissen, A. 2013, A&A, 557, A40
Dhillon, V. S., Privett, G. J., & Duffey, K. P. 2001, Starlink User Note 167.6 (Rutherford Appleton Laboratory)
Durand, S., Acker, A., & Zijlstra, A. 1998, A&AS, 132, 13
Epchtein, N., Deul, E., Derriere, S., et al. 1999, A&A, 349, 236
Ercolano, B., Barlow, M. J., Storey, P. J., & Liu, X.-W. 2003, MNRAS, 340, 1136
Exter, K. M., Pollacco, D. L., Maxted, P. F. L., Napiwotzki, R., & Bell, S. A. 2005, MNRAS, 359, 315
Ferguson, D. H., Liebert, J., Haas, S., Napiwotzki, R., & James, T. A. 1999, ApJ, 518, 866
García-Rojas, J. & Esteban, C. 2007, ApJ, 670, 457
Hamuy, M., Walker, A. R., Suntzeff, N. B., et al. 1992, PASP, 104, 533
Henize, K. G. 1967, ApJS, 14, 125
Hilditch, R. W., Harries, T. J., & Hill, G. 1996, MNRAS, 279, 1380
Hillwig, T. C., Bond, H. E., Afşar, M., & De Marco, O. 2010, AJ, 140, 319
Hillwig, T. C., Frew, D. J., Louie, M., et al. 2015, ApJ, in press
Horne, K. 1986, PASP, 98, 609
Howarth, I. D. 1983, MNRAS, 203, 301
Huckvale, L., Prouse, B., Jones, D., et al. 2013, MNRAS, 434, 1505
Jones, D. 2011, PhD thesis, Jodrell Bank Centre for Astrophysics, University of Manchester, UK
Jones, D., Boffin, H. M. J., Miszalski, B., et al. 2014a, A&A, 562, A89
Jones, D., Lloyd, M., Mitchell, D. L., et al. 2010a, MNRAS, 401, 405
Jones, D., Lloyd, M., Santander-García, M., et al. 2010b, MNRAS, 408, 2312
Jones, D., Mitchell, D. L., Lloyd, M., et al. 2012, MNRAS, 420, 2261
Jones, D., Santander-García, M., Boffin, H. M. J., Miszalski, B., & Corradi, R. L. M. 2014b, in Asymmetrical Planetary Nebulae VI Conference, 43
Kaler, J. B. & Jacoby, G. H. 1991, ApJ, 372, 215
Kingsburgh, R. L. & Barlow, M. J. 1994, MNRAS, 271, 257
Kobulnicky, H. A., Nordsieck, K. H., Burgh, E. B., et al. 2003, in Society of Photo-Optical Instrumentation Engineers (SPIE) Conference Series, Vol. 4841, Society of Photo-Optical Instrumentation Engineers (SPIE) Conference Series, ed. M. Iye & A. F. M. Moorwood, 1634–1644
Kurucz, R. L. 1993, VizieR Online Data Catalog, 6039, 0
Manick, R., Miszalski, B., & McBride, V. 2015, MNRAS, 448, 1789
Marsh, T. R. 1989, PASP, 101, 1032
Miszalski, B., Acker, A., Moffat, A. F. J., Parker, Q. A., & Udalski, A. 2008, A&A, 488, L79
Miszalski, B., Acker, A., Moffat, A. F. J., Parker, Q. A., & Udalski, A. 2009a, A&A, 496, 813
Miszalski, B., Acker, A., Parker, Q. A., & Moffat, A. F. J. 2009b, A&A, 505, 249
Miszalski, B., Boffin, H. M. J., & Corradi, R. L. M. 2013, MNRAS, 428, L39
Miszalski, B., Corradi, R. L. M., Boffin, H. M. J., et al. 2011a, MNRAS, 413, 1264

Miszalski, B., Jones, D., Rodríguez-Gil, P., et al. 2011b, A&A, 531, A158
Mitchell, D. L., Pollacco, D., O'Brien, T. J., et al. 2007, MNRAS, 374, 1404
Nordhaus, J. & Blackman, E. G. 2006, MNRAS, 370, 2004
O'Donoghue, D., Buckley, D. A. H., Balona, L. A., et al. 2006, MNRAS, 372, 151
Paxton, B., Bildsten, L., Dotter, A., et al. 2011, ApJS, 192, 3
Peimbert, M. 1978, in IAU Symposium, Vol. 76, Planetary Nebulae, ed. Y. Terzian, 215–223
Phillips, J. P. 2004, MNRAS, 353, 589
Preite-Martinez, A., Acker, A., Koeppen, J., & Stenholm, B. 1989, A&AS, 81, 309
Prialnik, D. & Livio, M. 1985, MNRAS, 216, 37
Reed, B. C. 1998, JRASC, 92, 36
Sahai, R., Morris, M. R., & Villar, G. G. 2011, AJ, 141, 134
Sandquist, E. L., Taam, R. E., Chen, X., Bodenheimer, P., & Burkert, A. 1998, ApJ, 500, 909
Santander-García, M., Rodríguez-Gil, P., Corradi, R. L. M., et al. 2015, Nature, 519, 63
Shimansky, V. V., Pozdnyakova, S. A., Borisov, N. V., et al. 2009, Astrophysical Bulletin, 64, 349
Snodgrass, C., Saviane, I., Monaco, L., & Sinclaire, P. 2008, The Messenger, 132, 18
Soker, N. & Rappaport, S. 2001, ApJ, 557, 256
Soker, N., Rappaport, S., & Harpaz, A. 1998, ApJ, 496, 842
Stanghellini, L., Shaw, R. A., & Villaver, E. 2008, ApJ, 689, 194
Tocknell, J., De Marco, O., & Wardle, M. 2014, MNRAS, 439, 2014
Tylenda, R., Siódmiak, N., Górny, S. K., Corradi, R. L. M., & Schwarz, H. E. 2003, A&A, 405, 627
Tyndall, A. A., Jones, D., Lloyd, M., O'Brien, T. J., & Pollacco, D. 2012, MNRAS, 422, 1804
van Dokkum, P. G. 2001, PASP, 113, 1420
Vassiliadis, E. & Wood, P. R. 1994, ApJS, 92, 125
Wesson, R., Barlow, M. J., Liu, X.-W., et al. 2008, MNRAS, 383, 1639
Wesson, R., Liu, X.-W., & Barlow, M. J. 2003, MNRAS, 340, 253
Wesson, R., Liu, X.-W., & Barlow, M. J. 2005, MNRAS, 362, 424
Wesson, R., Stock, D. J., & Scicluna, P. 2012, MNRAS, 422, 3516
Winget, D. E. & Kepler, S. O. 2008, ARA&A, 46, 157
Zhang, C. Y. 1995, ApJS, 98, 659

Table 2. A log of the Hβ-continuum photometric observations and measurements of the central star of Hen 2-155. Data also available in machine-readable format via anonymous ftp from CDS.

Julian Date	Exposure time (s)	Hβ-continuum magnitude	Uncertainty on Hβ-continuum magnitude
2455985.7989840	90	15.0020	0.0304
2455985.8008033	150	15.0008	0.0211
2455985.8029363	150	15.0086	0.0213
2455985.8050782	150	15.0051	0.0211
2455985.8517651	150	14.8521	0.0193
2455985.8538980	150	14.8548	0.0192
2455985.8560267	150	14.8768	0.0197
2455985.8928693	150	14.9180	0.0198
2455985.8950082	150	14.9041	0.0204
2455985.8971377	150	14.9504	0.0211
2455985.8994509	150	14.9460	0.0226
2455985.9015940	150	14.9688	0.0251
2455985.9038309	150	14.9632	0.0293
2455986.7685927	150	14.8737	0.0218
2455986.7707301	150	14.8869	0.0207
2455986.7728711	150	14.8874	0.0210
2455986.7988129	150	14.9825	0.0204
2455986.8009496	150	14.9838	0.0208
2455986.8030796	150	14.9842	0.0204
2455986.8424549	150	15.0068	0.0202
2455986.8445840	150	15.0109	0.0203
2455986.8467141	150	14.9983	0.0202
2455986.8633496	150	14.9380	0.0195
2455986.8654867	150	14.9186	0.0195
2455986.8676278	150	14.9227	0.0195
2455986.8989045	240	14.9124	0.0164
2455986.9020726	240	14.9053	0.0190
2455986.9052437	240	14.8986	0.0239
2455986.9084149	240	14.8684	0.0315
2455987.7737781	240	14.8719	0.0146
2455987.7769572	240	14.8459	0.0146
2455987.7801395	240	14.8638	0.0146
2455987.8287887	240	14.9516	0.0144
2455987.8319682	240	14.9647	0.0144
2455987.8351401	240	14.9805	0.0145
2455987.8557959	240	15.0370	0.0147
2455987.8589712	240	15.1094	0.0151
2455987.8621534	240	15.1781	0.0153
2455987.8739850	240	15.0048	0.0145
2455987.8771649	240	15.0116	0.0145
2455987.8803363	240	14.9912	0.0145
2455987.8835078	240	14.9943	0.0145
2455987.8866787	240	14.9822	0.0145
2455987.8898617	240	14.9740	0.0147
2455988.7545551	240	15.1696	0.0170
2455988.7577319	240	15.1223	0.0167
2455988.7609034	240	15.0451	0.0159
2455988.7640752	240	15.0063	0.0162
2455988.7672461	240	14.9884	0.0161
2455988.7704180	240	14.9918	0.0161
2455988.8775318	240	14.9880	0.0145
2455988.8807068	240	14.9985	0.0143
2455989.8336887	240	14.9151	0.0149
2455989.8368668	240	14.9035	0.0149
2455989.8400383	240	14.8980	0.0147
2455989.8693272	240	14.9338	0.0145
2455989.8725036	240	14.8726	0.0146
2455989.8885252	240	14.8834	0.0150
2455989.8917048	240	14.8988	0.0152

Table 2. continued.

Julian Date	Exposure time (s)	Hβ-continuum magnitude	Uncertainty on Hβ-continuum magnitude
2456712.7485850	240	14.9415	0.0183
2456712.7517599	240	14.9325	0.0181
2456712.7549312	240	14.9680	0.0176
2456712.7581045	240	14.9799	0.0180
2456712.7612776	240	14.9929	0.0173
2456712.7644514	240	14.9975	0.0174
2456712.7676246	240	15.0094	0.0172
2456712.7707959	240	15.0151	0.0173
2456712.7739676	240	15.0231	0.0173
2456712.7771418	240	15.0820	0.0175
2456712.7803185	240	15.1568	0.0179
2456712.7834991	240	15.1819	0.0183
2456712.7866744	240	15.1511	0.0178
2456712.7898470	240	15.0709	0.0174
2456712.7930182	240	14.9734	0.0170
2456712.7961942	240	14.9903	0.0171
2456712.7993699	240	14.9847	0.0171
2456712.8025435	240	14.9925	0.0169
2456712.8057199	240	14.9825	0.0170
2456712.8088957	240	14.9828	0.0168
2456712.8120692	240	14.9572	0.0168
2456712.8152405	240	14.9514	0.0166
2456712.8184117	240	14.9383	0.0165
2456712.8215838	240	14.9182	0.0166
2456712.8247545	240	14.9205	0.0165
2456712.8279307	240	14.9028	0.0165
2456712.8311070	240	14.8989	0.0166
2456712.8342797	240	14.8942	0.0164
2456712.8406225	240	14.8618	0.0164
2456712.8437979	240	14.8639	0.0161
2456712.8469705	240	14.8600	0.0160
2456712.8501450	240	14.8620	0.0162
2456712.8533192	240	14.8933	0.0162
2456712.8564960	240	14.9120	0.0165
2456712.8596705	240	14.8935	0.0167
2456712.8628436	240	14.8747	0.0162
2456712.8660158	240	14.8529	0.0164
2456712.8691906	240	14.8621	0.0162
2456712.8723667	240	14.8753	0.0162
2456712.8755420	240	14.8705	0.0164
2456712.8787159	240	14.8787	0.0164
2456712.8818900	240	14.8844	0.0166
2456712.8850649	240	14.9206	0.0167
2456712.8882415	240	14.9155	0.0174
2456712.8914157	240	14.9155	0.0178
2456712.8945906	240	14.9171	0.0192
2456712.8977621	240	14.9348	0.0214
2456713.7694692	240	14.8799	0.0166
2456713.7821596	240	14.9281	0.0161
2456713.8051735	240	14.9982	0.0167
2456713.8197508	240	15.1681	0.0180
2456713.8229228	240	15.1603	0.0178
2456713.8260968	240	15.1091	0.0173
2456713.8292670	240	15.0124	0.0173
2456713.8324438	240	14.9939	0.0172
2456713.8620228	240	14.9088	0.0163
2456713.8801730	240	14.8479	0.0157
2456714.8685630	240	14.9932	0.0162
2456715.7739455	240	14.9621	0.0155
2456715.8354988	240	14.8502	0.0155

Table 3. A log of the *I*-band photometric observations and measurements of the central star of Hen 2-161. Observations marked with an asterisk are from the SAAO 1.0-m telescope taken with a Cousins *I*-band filter, all other observations were acquired with NTT-EFOSC2 and a Gunn *i* filter (see text for further details). Data also available in machine-readable format via anonymous ftp from CDS.

Julian Date	Exposure time (s)	*I*-band magnitude	Uncertainty on *I*-band magnitude
2455987.7904517	45	15.2006	0.0120
2455987.7913786	45	15.1932	0.0121
2455987.7923043	45	15.2113	0.0120
2455987.8456948	45	15.1422	0.0117
2455987.8466095	45	15.1478	0.0116
2455987.8475239	45	15.1570	0.0116
2455987.8698281	45	15.1316	0.0111
2455987.8707530	45	15.1248	0.0111
2455987.8716673	45	15.1235	0.0113
2455988.7951585	45	15.1798	0.0124
2455988.7960771	45	15.1748	0.0124
2455988.7969902	45	15.1782	0.0126
2455988.7979061	45	15.1776	0.0129
2455988.7988199	45	15.1794	0.0125
2455988.8284592	45	15.1464	0.0126
2455988.8293755	45	15.1623	0.0116
2455988.8302899	45	15.1612	0.0120
2455988.8312045	45	15.1596	0.0114
2455988.8321303	45	15.1264	0.0132
2455988.8330565	45	15.1494	0.0123
2455988.8339706	45	15.1570	0.0122
2455988.8734464	45	15.1181	0.0112
2455988.8743642	45	15.1114	0.0120
2455988.8752783	45	15.1063	0.0112
2455988.9092162	45	15.0767	0.0197
2455988.9101280	45	15.0795	0.0213
2455988.9110539	45	15.0908	0.0236
2455988.9120965	45	15.0711	0.0253
2455988.9130097	45	15.0559	0.0293
2455988.9139242	45	15.0799	0.0310
2455989.7756987	60	15.1787	0.0110
2455989.7767974	60	15.1788	0.0111
2455989.7779935	60	15.1741	0.0115
2455989.7790776	60	15.1792	0.0113
2455989.8118550	60	15.1520	0.0111
2455989.8129437	60	15.1667	0.0112
2455989.8140312	60	15.1646	0.0114
2455989.8151193	60	15.1451	0.0123
2455989.8162188	60	15.1596	0.0115
2455989.8173181	60	15.1532	0.0117
2455989.8184179	60	15.1484	0.0115
2455989.8195056	60	15.1611	0.0108
2455989.8205937	60	15.1574	0.0113
2455989.8216820	60	15.1506	0.0114
2455989.8542936	60	15.1465	0.0097
2455989.8553856	60	15.1463	0.0097
2455989.8564737	60	15.1477	0.0095
2455989.8575615	60	15.1357	0.0099
2455989.8586609	60	15.1436	0.0096
∗ 2456020.4300300	90	15.0213	0.0239
∗ 2456020.4317400	90	14.9752	0.0243
∗ 2456020.4334400	90	14.9865	0.0245
∗ 2456020.4351400	90	14.9703	0.0245
∗ 2456020.4368300	90	15.0060	0.0237
∗ 2456020.4385300	90	15.0092	0.0241
∗ 2456020.4643600	90	15.0226	0.0227
∗ 2456020.4660600	90	15.0153	0.0236
∗ 2456020.4677700	90	15.0053	0.0238

Table 3. continued.

Julian Date	Exposure time (s)	*I*-band magnitude	Uncertainty on *I*-band magnitude
∗ 2456020.4694800	90	14.9978	0.0236
∗ 2456020.4711700	90	15.0191	0.0236
∗ 2456020.4728700	90	14.9946	0.0233
∗ 2456020.5401500	90	14.9814	0.0227
∗ 2456020.5418500	90	15.0005	0.0222
∗ 2456020.5437800	90	14.9933	0.0242
∗ 2456020.5453100	90	15.0016	0.0240
∗ 2456020.5468400	90	14.9933	0.0242
∗ 2456020.5483700	90	14.9922	0.0243
∗ 2456020.5498800	90	14.9934	0.0245
∗ 2456020.5514200	90	15.0069	0.0239
2456308.8388791	60	15.1144	0.0122
2456308.8399697	60	15.0490	0.0131
2456308.8410683	60	15.0941	0.0129
2456712.9020590	60	15.0705	0.0138
2456712.9031510	60	15.0727	0.0153
2456712.9042402	60	15.0441	0.0162
2456712.9064182	60	15.0333	0.0193
2456712.9075069	60	15.1185	0.0211
2456712.9085973	60	15.0293	0.0223
2456713.7874744	30	15.1397	0.0132
2456713.8696886	30	15.1325	0.0098
2456713.8707783	30	15.1018	0.0101
2456713.8718675	30	15.1009	0.0103
2456713.8729605	30	15.0926	0.0137
2456713.8736989	30	15.0973	0.0111
2456713.8746154	30	15.0968	0.0131
2456713.8753560	30	15.0826	0.0134
2456713.9050826	30	15.0255	0.0170
2456713.9058287	30	15.0434	0.0173
2456713.9065719	30	15.0360	0.0183
2456713.9073110	30	15.0348	0.0191
2456713.9080531	30	15.0387	0.0196
2456713.9087938	30	15.0381	0.0211
2456713.9095347	30	15.0664	0.0221
2456713.9102812	30	15.0268	0.0239
2456713.9110239	30	15.0735	0.0246
2456713.8366994	30	15.1993	0.0138
2456713.8377933	30	15.0824	0.0128
2456713.8388863	30	15.1242	0.0128
2456715.7651854	30	15.1765	0.0139
2456715.7659303	30	15.1752	0.0139
2456715.7666715	30	15.1780	0.0141
2456715.7674132	30	15.1861	0.0139
2456715.7681527	30	15.1853	0.0139
2456715.7688957	30	15.1679	0.0139
2456715.7696373	30	15.1724	0.0139
2456715.7703794	30	15.1717	0.0137
2456715.7711246	30	15.1757	0.0137
2456715.7718605	30	15.1818	0.0138
2456715.7821279	30	15.1772	0.0142
2456715.7828718	30	15.1800	0.0138
2456715.7836141	30	15.1942	0.0138
2456715.7843573	30	15.1833	0.0135
2456715.7851024	30	15.1680	0.0142
2456715.7997002	30	15.1677	0.0136
2456715.8004471	30	15.1670	0.0138
2456715.8011896	30	15.1870	0.0134
2456715.8019356	30	15.1745	0.0136
2456715.8026814	30	15.1713	0.0134

Table 3. continued.

Julian Date	Exposure time (s)	*I*-band magnitude	Uncertainty on *I*-band magnitude
2456715.8163368	30	15.1464	0.0140
2456715.8170778	30	15.1751	0.0135
2456715.8178196	30	15.1611	0.0137
2456715.8185615	30	15.1565	0.0140
2456715.8193035	30	15.1515	0.0138
2456715.8275854	30	15.1554	0.0134
2456715.8283297	30	15.1479	0.0132
2456715.8290752	30	15.1623	0.0133
2456715.8298200	30	15.1427	0.0135
2456715.8305639	30	15.1541	0.0134
2456715.8397072	30	15.1192	0.0143
2456715.8404538	30	15.1482	0.0155
2456715.8411984	30	15.0934	0.0155
2456715.8419406	30	15.1156	0.0141
2456715.8426877	30	15.1134	0.0145
2456715.8553575	30	15.1016	0.0138
2456715.8561049	30	15.1108	0.0140
2456715.8568454	30	15.1145	0.0139
2456715.8575932	30	15.1190	0.0139
2456715.8583346	30	15.1140	0.0139
2456715.8657918	30	15.0939	0.0147
2456715.8665369	30	15.0773	0.0140
2456715.8672778	30	15.0757	0.0143
2456715.8680232	30	15.0826	0.0139
2456715.8687678	30	15.1047	0.0136
2456715.8783854	30	15.0929	0.0130
2456715.8791289	30	15.0793	0.0133
2456715.8798703	30	15.0834	0.0130
2456715.8806149	30	15.1066	0.0131
2456715.8813587	30	15.1092	0.0125
2456715.8821031	30	15.1071	0.0124
2456715.8828448	30	15.1102	0.0128
2456715.8835893	30	15.1065	0.0126
2456715.8843321	30	15.1066	0.0124
2456715.8850763	30	15.1189	0.0122
2456715.8858229	30	15.1100	0.0121
2456715.8865687	30	15.1047	0.0123
2456715.8873128	30	15.1171	0.0122
2456715.8880534	30	15.1035	0.0122
2456715.8887966	30	15.0976	0.0124
2456715.8895430	30	15.0848	0.0124
2456715.8902869	30	15.1029	0.0124
2456715.8910275	30	15.0973	0.0123
2456715.8917722	30	15.0993	0.0123
2456715.8925178	30	15.1040	0.0122
2456715.9027146	30	15.0835	0.0153
2456715.9034564	30	15.0735	0.0163
2456715.9041989	30	15.0818	0.0175
2456715.9049431	30	15.0771	0.0177
2456715.9056870	30	15.0840	0.0185
2456715.9064324	30	15.0778	0.0197
2456715.9071736	30	15.0769	0.0213
2456715.9079143	30	15.0791	0.0226
2456715.9086595	30	15.0533	0.0239
2456715.9094049	30	15.0890	0.0262
2456715.9101482	30	15.0866	0.0282
2456715.9108930	30	15.0884	0.0302
2456715.9116378	30	15.1014	0.0315
2456715.9123814	30	15.0818	0.0346
2456715.9131226	30	15.0021	0.0391

Table 3. continued.

Julian Date	Exposure time (s)	*I*-band magnitude	Uncertainty on *I*-band magnitude
2456715.9138636	30	15.1047	0.0445
2456715.9146030	30	15.1301	0.0470
2456715.9153486	30	15.1707	0.0530

Table 4. A log of the radial velocity measurements of the central star of Hen 2-155. Data also available in machine-readable format via anonymous ftp from CDS.

Julian Date	Radial Velocity (km s^{-1})	Uncertainty on radial velocity (km s^{-1})
2456371.7604575	-27.9696	2.8980
2456371.7720789	-50.7702	3.4633
2456371.7837002	-63.7826	3.3738
2456371.7953216	-53.4388	3.7784
2456371.8069431	-29.0446	3.2967
2456371.8185528	-8.8539	2.5652
2456371.8301742	23.8644	2.7731
2456371.8417956	50.8250	2.5643
2456371.8534171	56.5280	2.4353
2456371.8650384	59.9633	3.1728
2456371.8766599	35.6776	3.4437
2456371.8882813	15.7247	2.7868
2456371.9016389	-18.8627	2.6239

Table 5. A log of the radial velocity measurements of the C IV lines of Hen 2-155. Data also available in machine-readable format via anonymous ftp from CDS.

Julian Date	Radial Velocity (km s^{-1})	Uncertainty on radial velocity (km s^{-1})
2456371.7604575	-20.5399	2.7514
2456371.7720789	-22.5216	2.6793
2456371.7837002	-35.5964	3.2085
2456371.7953216	-38.9358	2.9990
2456371.8069431	-24.4214	2.5088
2456371.8185528	2.7566	5.1585
2456371.8301742	7.9988	3.1546
2456371.8417956	19.2400	3.2090
2456371.8534171	31.3309	2.4482
2456371.8650384	36.1928	3.1091
2456371.8766599	21.5965	2.6399
2456371.8882813	19.7743	2.4719
2456371.9016389	6.1171	2.5737

Table 6. Observed, $F(\lambda)$, and dereddened, $I(\lambda)$, nebular emission line fluxes from Hen 2-155 and Hen 2-161

		Hen2-155				Hen2-161			
λ (Å)	Ion	$F(\lambda)$		$I(\lambda)$		$F(\lambda)$		$I(\lambda)$	
3664.68	H I	0.28	± 0.05	0.43	$^{+0.07}_{-0.08}$	-	-	-	-
3666.10	H I	0.26	± 0.05	0.38	$^{+0.07}_{-0.08}$	0.41	± 0.08	0.85	$^{+0.14}_{-0.17}$
3667.68	H I	-		-		0.20	± 0.05	0.26	$^{+0.05}_{-0.06}$
3669.46	H I	0.26	± 0.08	0.42	$^{+0.09}_{-0.11}$	-	-	-	-
3709.62	Ne II	-		-		0.27	± 0.05	0.53	$^{+0.09}_{-0.11}$
3711.97	H I	0.64	± 0.07	1.00	± 0.11	0.84	± 0.08	1.72	± 0.15
3713.08	Ne II	0.35	± 0.08	0.48	$^{+0.09}_{-0.11}$	-	-	-	-
3721.94	H I	1.50	± 0.14	2.33	± 0.21	1.07	± 0.13	2.20	± 0.27
3726.03	[O II]	15.55	± 0.15	24.07	± 0.24	8.81	± 0.10	18.02	± 0.23
3728.82	[O II]	11.60	± 0.16	17.94	± 0.25	5.70	± 0.08	11.64	± 0.18
3734.37	H I	1.36	± 0.09	2.10	± 0.13	0.97	± 0.07	1.98	± 0.14
3750.15	H I	1.92	± 0.04	2.95	± 0.06	1.28	± 0.04	2.58	± 0.08
3770.63	H I	2.20	± 0.07	3.36	± 0.11	1.52	± 0.09	3.03	± 0.18
3797.90	H I	2.90	± 0.08	4.39	± 0.12	1.97	± 0.11	3.89	± 0.22
3856.13	O II	-		-		0.17	± 0.05	0.25	$^{+0.05}_{-0.07}$
3868.75	[Ne III]	56.77	± 0.08	84.06	± 0.21	15.38	± 0.13	29.23	± 0.28
3888.65	He I	9.10	± 0.05	13.38	± 0.08	7.47	± 0.06	14.05	± 0.14
3889.05	H I	5.36	± 0.06	7.88	± 0.08	4.35	± 0.07	8.17	± 0.14
3964.73	He I	-		-		0.70	± 0.15	1.16	$^{+0.20}_{-0.25}$
3967.46	[Ne III]	17.56	± 0.27	25.13	± 0.39	4.48	± 0.15	8.06	± 0.27
3970.07	H I	9.36	± 0.26	13.38	± 0.38	6.92	± 0.13	12.43	± 0.25
4026.21	He I	1.42	± 0.03	1.99	± 0.04	1.48	± 0.04	2.57	± 0.08
4068.60	[S II]	0.39	± 0.02	0.54	± 0.02	0.28	± 0.03	0.47	± 0.04
4069.62	O II	0.26	± 0.01	0.37	± 0.02	0.31	± 0.03	0.53	± 0.04
4072.16	O II	0.24	± 0.01	0.32	± 0.02	0.38	± 0.03	0.63	± 0.05
4075.86	O II	0.30	± 0.02	0.42	± 0.03	0.39	± 0.03	0.65	± 0.06
4076.35	[S II]	0.17	± 0.02	0.23	± 0.03	-		-	
4078.84	O II	0.06	± 0.02	0.06	$^{+0.01}_{-0.02}$	-		-	
4085.11	O II	0.07	± 0.02	0.08	± 0.02	-		-	
4087.15	O II	-		-		0.19	± 0.03	0.31	$^{+0.05}_{-0.06}$
4089.29	O II	0.15	± 0.02	0.20	± 0.03	0.41	± 0.03	0.69	± 0.04
4097.26	O II	0.79	± 0.06	1.07	± 0.08	0.36	± 0.04	0.59	± 0.07
4101.74	H I	17.93	± 0.06	24.44	± 0.09	15.00	± 0.04	24.88	± 0.13
4120.28	O II	0.13	± 0.02	0.17	± 0.03	-		-	
4121.46	O II	0.17	± 0.05	0.23	$^{+0.04}_{-0.06}$	-		-	
4132.80	O II	0.08	± 0.02	0.09	± 0.02	-		-	
4153.30	O II	0.11	± 0.02	0.14	$^{+0.02}_{-0.03}$	0.22	± 0.03	0.35	± 0.05
4156.53	O II	-		-		0.13	± 0.03	0.18	$^{+0.03}_{-0.04}$
4186.90	C III	0.09	± 0.02	0.12	± 0.02	-		-	
4237.05	N II	-		-		0.10	± 0.02	0.15	± 0.02
4241.78	N II	-		-		0.10	± 0.02	0.15	$^{+0.02}_{-0.03}$
4267.15	C II	0.24	± 0.01	0.30	± 0.01	1.56	± 0.03	2.34	± 0.04
4273.10	O II	0.04	± 0.01	0.03	± 0.01	-		-	
4275.55	O II	0.04	± 0.01	0.04	± 0.01	-		-	
4276.75	O II	-		-		0.12	± 0.01	0.18	± 0.02
4275.99	O II	0.03	± 0.01	0.03	± 0.01	-		-	
4277.89	O II	-		-		0.10	± 0.01	0.15	± 0.02
4282.96	O II	-		-		0.07	± 0.01	0.11	± 0.02
4285.69	O II	-		-		0.06	± 0.01	0.09	$^{+0.01}_{-0.02}$
4291.25	O II	0.03	± 0.01	0.03	± 0.01	-		-	
4294.78	O II	0.05	± 0.01	0.06	± 0.01	0.09	± 0.01	0.13	± 0.02
4303.61	O II	0.11	± 0.01	0.13	± 0.01	0.17	± 0.03	0.25	± 0.04
4317.14	O II	-		-		0.16	± 0.02	0.24	± 0.02
4317.70	O II	-		-		0.05	± 0.02	0.06	$^{+0.01}_{-0.02}$
4319.63	O II	-		-		0.10	± 0.02	0.15	± 0.02
4340.47	H I	34.68	± 0.08	43.04	± 0.12	32.08	± 0.17	45.67	± 0.29
4345.55	O II	-		-		0.45	± 0.08	0.63	$^{+0.10}_{-0.12}$
4349.43	O II	0.12	± 0.02	0.14	$^{+0.02}_{-0.03}$	0.29	± 0.05	0.40	$^{+0.07}_{-0.08}$

Table 6. continued.

		Hen2-155				Hen2-161			
λ (Å)	Ion	$F(\lambda)$		$I(\lambda)$		$F(\lambda)$		$I(\lambda)$	
4363.21	[O III]	5.67	± 0.02	6.97	± 0.03	0.60	± 0.03	0.84	± 0.04
4366.89	O II	0.09	± 0.02	0.09	± 0.02	0.23	± 0.02	0.32	± 0.03
4379.11	N III	0.16	± 0.01	0.20	± 0.02	0.09	± 0.03	0.09	$^{+0.02}_{-0.03}$
4387.93	He I	0.47	± 0.01	0.57	± 0.01	0.54	± 0.03	0.75	± 0.03
4416.97	O II	-		-		0.10	± 0.03	0.12	$^{+0.02}_{-0.03}$
4437.55	He I	0.04	± 0.01	0.03	± 0.01	-		-	
4452.37	O II	0.04	± 0.01	0.04	± 0.01	0.16	± 0.04	0.18	$^{+0.03}_{-0.04}$
4471.50	He I	4.21	± 0.02	4.96	± 0.03	4.91	± 0.06	6.41	± 0.08
4530.41	N II	-		-		0.06	± 0.02	0.07	$^{+0.01}_{-0.02}$
4552.53	N II	0.05	± 0.02	0.05	± 0.01	-		-	
4601.48	N II	0.07	± 0.01	0.08	± 0.01	-		-	
4609.44	O II	0.03	± 0.01	0.03	± 0.01	0.13	± 0.02	0.15	± 0.02
4610.20	O II	0.06	± 0.01	0.06	± 0.01	-		-	
4630.54	N II	0.06	± 0.02	0.06	± 0.01	0.20	± 0.03	0.23	± 0.03
4640.64	N III	0.77	± 0.02	0.85	± 0.02	0.53	± 0.02	0.61	± 0.02
4647.42	C III	0.08	± 0.01	0.09	± 0.01	-		-	
4649.13	O II	0.37	± 0.01	0.40	± 0.02	0.87	± 0.03	1.00	± 0.04
4650.25	C III	0.04	± 0.01	0.03	± 0.01	-		-	
4650.84	O II	0.11	± 0.01	0.12	± 0.02	0.20	± 0.03	0.23	± 0.04
4661.63	O II	0.14	± 0.01	0.16	± 0.02	0.32	± 0.02	0.36	± 0.02
4685.68	He II	7.45	± 0.03	8.02	± 0.04	0.45	± 0.10	0.46	$^{+0.08}_{-0.10}$
4696.35	O II	-		-		0.08	± 0.03	0.07	± 0.02
4711.37	[Ar IV]	2.32	± 0.02	2.47	± 0.03	0.34	± 0.04	0.37	± 0.05
4713.17	He I	0.38	± 0.02	0.41	± 0.02	0.45	± 0.04	0.50	± 0.05
4714.17	[Ne IV]	0.07	± 0.02	0.06	± 0.01	-		-	
4725.62	[Ne IV]	-		-		0.07	± 0.02	0.06	± 0.01
4740.17	[Ar IV]	1.85	± 0.03	1.95	± 0.03	0.22	± 0.05	0.21	$^{+0.04}_{-0.05}$
4861.33	H I	100.00	± 0.13	100.00	±0.15	100.00	± 0.29	100.00	± 0.30
4906.83	O II	-		-		0.12	± 0.02	0.12	± 0.02
4921.93	He I	1.42	± 0.04	1.38	± 0.04	1.70	± 0.03	1.63	± 0.03
4924.53	O II	-		-		0.16	± 0.03	0.14	$^{+0.02}_{-0.03}$
4958.91	[O III]	238.20	± 2.22	228.68	± 2.15	101.91	± 0.32	95.33	± 0.40
5006.84	[O III]	-		-		303.14	± 2.03	274.44	± 1.99
5015.68	He I	4.15	± 0.84	3.63	$^{+0.62}_{-0.75}$	-		-	
5754.60	[N II]	-		-		1.08	± 0.10	0.63	± 0.06
5875.66	He I	-		-		34.56	± 0.25	19.00	± 0.14
5931.78	N II	0.23	± 0.07	0.12	± 0.03	0.33	± 0.09	0.15	± 0.03
5941.65	N II	0.27	± 0.07	0.16	$^{+0.03}_{-0.04}$	0.25	± 0.07	0.11	$^{+0.02}_{-0.03}$
6312.10	[S III]	2.39	± 0.07	1.47	± 0.04	0.92	± 0.10	0.42	± 0.04
6461.95	C II	0.13	± 0.02	0.08	$^{+0.01}_{-0.02}$	0.52	± 0.07	0.22	± 0.03
6548.10	[N II]	22.72	± 0.11	13.22	± 0.07	34.66	± 0.30	14.29	± 0.13
6562.77	H I	478.84	± 0.66	277.58	± 0.17	705.65	± 1.16	289.19	± 0.35
6583.50	[N II]	69.02	± 0.25	39.81	± 0.15	106.91	± 0.53	43.46	± 0.23
6678.16	He I	7.34	± 0.07	4.14	± 0.04	13.15	± 0.08	5.15	± 0.03
6716.44	[S II]	9.49	± 0.08	5.30	± 0.05	10.80	± 0.15	4.17	± 0.06
6730.82	[S II]	11.60	± 0.09	6.46	± 0.05	13.74	± 0.16	5.28	± 0.06
7065.25	He I	6.85	± 0.34	3.54	± 0.18	3.18	± 0.38	1.08	± 0.13
7135.80	[Ar III]	26.68	± 1.39	13.58	± 0.71	33.00	± 0.16	10.94	± 0.06